Geophysical Journal International

*Geophys. J. Int.* (2011) **184,** 1090–1112 doi: 10.1111/j.1365-246X.2010.04919.x



# Pervasive Palaeogene remagnetization of the central Taurides fold-and-thrust belt (southern Turkey) and implications for rotations in the Isparta Angle

Maud J. M. Meijers,[1,2]* Douwe J. J. van Hinsbergen,[3] Mark J. Dekkers,[1] Demir Altıner,[4] Nuretdin Kaymakcı[4] and Cor G. Langereis[1]

[1] *Palaeomagnetic Laboratory Fort Hoofddijk, Dept. of Earth Sciences, Utrecht University, Budapestlaan* 17, 3584 *CD Utrecht, The Netherlands. E-mail: meijers@geo.uu.nl*

[2] *Dept. of Tectonics and Structural Geology, Faculty of Earth and Life Sciences, VU University Amsterdam, De Boelelaan* 1085, 1081 *HV Amsterdam, The Netherlands*

[3] *Physics of Geological Processes (PGP), University of Oslo, Physics building, Sem Sælands vei* 24, 0316 *Oslo, Norway*

[4] *Dept. of Geological Engineering, Faculty of Engineering, Middle East Technical University, İnönü Bulvarı*, 06531-*Ankara, Turkey*

Accepted 2010 December 9. Received 2010 December 6; in original form 2010 March 12

## SUMMARY

The Turkish Anatolide–Tauride block rifted away from the northern margin of Gondwana in the Triassic, which gave way to the opening of the southern Neo-Tethys. By the late Palaeocene to Eocene, it collided with the southern Eurasian margin, leading to the closure of the northern Neo-Tethys ocean. To determine the position of the Anatolide–Tauride block with respect to the African and Eurasian margin we carried out a palaeomagnetic study in the central Taurides belt, which constitutes the eastern limb of the Isparta Angle. The sampled sections comprise Carboniferous to Palaeocene rocks (mainly limestones). Our data suggest that all sampled rocks are remagnetized during the late Palaeocene to Eocene phase of folding and thrusting event, related to the collision of the Anatolide–Tauride block with Eurasia. To further test the possibility of remagnetization, we use a novel end-member modelling approach on 174 acquired isothermal remanent magnetization (IRM) curves. We argue that the preferred three end-member model confirms the proposed remagnetization of the rocks. Comparing our data to the post-Eocene declination pattern in the central Tauride belt, we conclude that our clockwise rotations are in agreement with data from other studies. After combining our results with previously published data from the Isparta Angle (that includes our study area), we have reasons to cast doubt on the spatial and temporal extent of an earlier reported early to middle Miocene remagnetization event. We argue that the earlier reported remagnetized directions from Triassic rocks—in tilt corrected coordinates—from the southwestern Antalya Nappes (western Taurides), are in good agreement with other studies from the area that show a primary origin of their characteristic remanent magnetization. This implies that we document a clockwise rotation for the southwestern Antalya Nappes since the Triassic that is remarkably similar to the post-Eocene (∼40°) rotation of the central Taurides. For the previously published results that are clearly remagnetized, we argue that their remagnetization has occurred in the Palaeocene to Eocene.

**Key words:** Palaeomagnetism applied to Tectonics; Remagnetization; Rock and mineral magnetism; Oceanic plateaus and microcontinents; Asia.

## 1 INTRODUCTION

Rifting and subduction of the Tethys oceans led to the northward drift of continental blocks away from the Gondwanan margin and their accretion to the Eurasian margin in Mesozoic times (Şengör & Yilmaz 1981). Palaeomagnetism is a widely used technique to reconstruct palaeolatitudes of accreted terranes and their vertical-block rotations. Turkey exposes such a terrane: the Anatolide–Tauride block (ATB). It is a continental fragment that rifted away from Gondwana in the early Mesozoic (Fig. 1; Şengör & Yilmaz 1981; Kröner & Şengör 1990; Hetzel & Reischmann 1996; Gessner *et al*. 2004) and it collided with the southern margin

*Now at: GéoAzur, UMR 6526, Université de Nice Sophia Antipolis, Parc Valrose, 06108 Nice, Cedex 2, France.

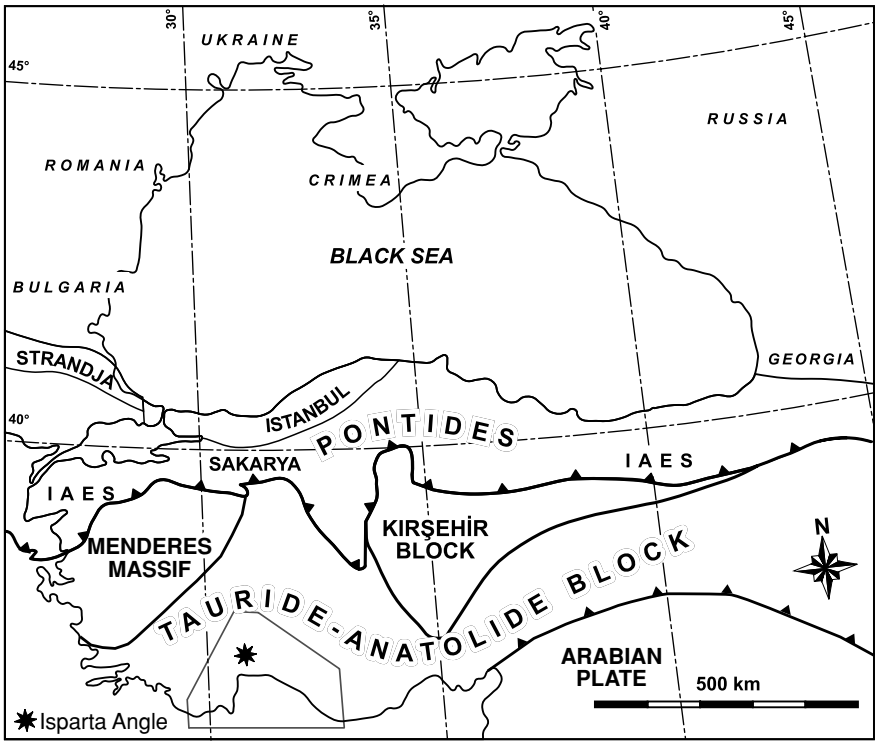


**Figure 1. (**a) Map showing the Taurides in the circum-Black Sea region. IAES, İzmir–Ankara–Erzincan suture zone. Grey box indicates the position of Figs 2(a)–(c).

of Eurasia in late Cretaceous to Palaeocene times (Okay *et al*. 2001; Kaymakci *et al*. 2009; van Hinsbergen *et al*. 2010c; Meijers *et al*. 2010). The analysis of timing and rates of opening and closing of the Tethys oceans that accommodated the northward drift of the ATB from Gondwana to Eurasia is essential to reconstruct its plate tectonic history. The available published reconstruction scenarios rely mainly on geological interpretations of the relict, intensely deformed rocks and pre-Alpine basement that are now exposed within the collision zone. Dissimilarity of most of the proposed models related to the position of the ATB with respect to the African margin from Permian to Jurassic times (Şengör & Yilmaz 1981; Şengör 1984; Stampfli & Borel 2002; Robertson *et al*. 2004; Moix *et al*. 2008; Mackintosh & Robertson 2009) indicate that there is large degree of freedom in the interpretations, which is mainly due to a lack of reliable data to constrain palaeopositions of the tectonic blocks of interest.

In this contribution, we aimed at constraining the palaeolatitudinal position of the ATB and its position with respect to the African and Eurasian margins. We conducted a palaeomagnetic study for the Carboniferous to Eocene stratigraphy of the central Tauride fold-and-thrust belt, to add data and to fill the gaps in the existing palaeomagnetic data (Van der Voo & Van der Kleijn 1970; Gallet *et al*. 1992, 1993, 1994, 1996, 2000; Piper *et al*. 2002). We must conclude however, that such a palaeolatitude reconstruction is not possible due to a regional, pervasive remagnetization event that reset the magnetic record in the central Taurides fold-and-thrust belt. We conclude from our data that this remagnetization event took place in the Palaeogene. In addition, we discuss the implications of this finding within the context of previous discussions related to cause and timing of the remagnetization event (Morris & Robertson 1993; van Hinsbergen *et al*. 2010b), as well as regional block rotation scenarios of the central Taurides (Kissel *et al*. 1993; Piper *et al*. 2002). We will discuss the implications of our findings for previous palaeomagnetic studies and the regional rotational scenarios that were inferred from them.

## 2 GEOLOGICAL BACKGROUND

The ATB in southern Turkey is of peri-Gondwanan origin, indicated by palaeontological data and its pre-Alpine basement (Satır & Friedrichsen 1986; Şengör *et al*. 1988; Kröner & Şengör 1990). The ATB is separated from the northward located Pontides, which are of Eurasian affinity, by the İzmir–Ankara–Erzincan suture zone (Fig. 1; Şengör & Yilmaz 1981). It is separated from the African continent by the still-subducting Levantine lithosphere (along the Hellenic–Cyprian trenches), which is likely of oceanic nature (Khair & Tsokas 1999). Generally it is accepted that after the assemblage of Pangea at the end of the Palaeozoic, a large triangular oceanic domain (the Palaeo-Tethys ocean) occupied the area between the Eurasian and Gondwanan margins (Şengör 1984). Palaeogeographic models related to the size, evolutionary history and subduction polarity of the Palaeo-Tethys vary widely (Şengör & Yilmaz 1981; Robertson *et al*. 2004; Moix *et al*. 2008). However, subduction of Palaeo-Tethys gave way to rifting off of continental blocks from the northern margin of Gondwana and to the opening of the Neo-Tethys ocean during the Mesozoic. Estimates on timing of opening of the southern Neo-Tethys ocean between Africa and the ATB vary from late Permian to early Triassic (Stampfli & Borel 2002; Moix *et al*. 2008), Triassic (Robertson *et al*. 2004) to late Triassic (Şengör & Yilmaz 1981; Şengör 1984). There is however a general consensus that from late Jurassic to late Cretaceous times the stratigraphic units of the Taurides developed as a passive margin, reflected by platform and shelf carbonates (Özgül 1976; Monod 1977; Gutnic *et al*. 1979).

During the late Cretaceous (∼90–80 Ma), the ATB was incorporated into the subduction system and obducted by ophiolites that

originated from northwards subduction of the Neo-Tethys. During the Palaeocene to early Eocene it collided with the Pontides after northern Neo-Tethys closure. This resulted in the development of a fold-and-thrust belt that is presently exposed in the Tauride mountain belt (Şengör & Yilmaz 1981; Okay *et al*. 2001; Çelik *et al*. 2006; Elitok & Drüppel 2008; Bağcı & Parlak 2009; Kaymakci *et al*. 2009; Robertson *et al*. 2009). The ATB is separated from the Pontides by two major crystalline massifs—the Menderes Massif in the west and the Central Anatolian Crystalline Complex or Kırşehir Block in central Turkey (Şengör & Yilmaz 1981; Okay *et al*. 1996). These two complexes are known as the Anatolides and are generally regarded as the metamorphosed northern extension of the ATB, which was obducted, metamorphosed and thrusted during the late Cretaceous to early Palaeogene (Okay *et al*. 2001; Kaymakci *et al*. 2009; Robertson *et al*. 2009). The degree of metamorphism within the Central Anatolian Crystalline Complex decreases southwards which indicates southward obduction and thrusting. The Taurides (*sensu stricto*) refer to the southern unmetamorphosed part of the ATB.

The Taurides comprise sedimentary sequences ranging in age from Cambrian to Tertiary, mostly composed of shallow marine platform type carbonates (Özgül 1976; Monod 1977; Şengör & Yilmaz 1981; Altıner *et al*. 1999; Dean *et al*. 1999; Özer *et al*. 2004; Mackintosh & Robertson 2009). The Taurides consist of several isopic units (Fig. 2) that are overthrusted and stacked as nappe sequences, mainly during the late Cretaceous to Oligocene (Andrew & Robertson 2002; Özer *et al*. 2004). Palaeogeographically, these isopic zones include (from south to north) the Antalya, Alanya, Geyikdağı, Aladağ, Bolkardağı and Bozkır units. The Geyikdağı unit is structurally the lowest and relatively autochtonous unit (Fig. 2). Because of its similar structural position and stratigraphy, the unmetamorphosed and mildly deformed Beydağları unit is generally considered as the lateral equivalent of the parautochthonous Geyikdağı unit (Özgül 1976). In general, the Geyikdağı unit is overthrusted by the Aladağ, Bolkardağ and Bozkır units from the north (Figs 2 and 3). The position and emplacement direction of the Antalya and Alanya units, however, is a matter of debate. The different models include: (1) all the nappes originated from the north (Ricou

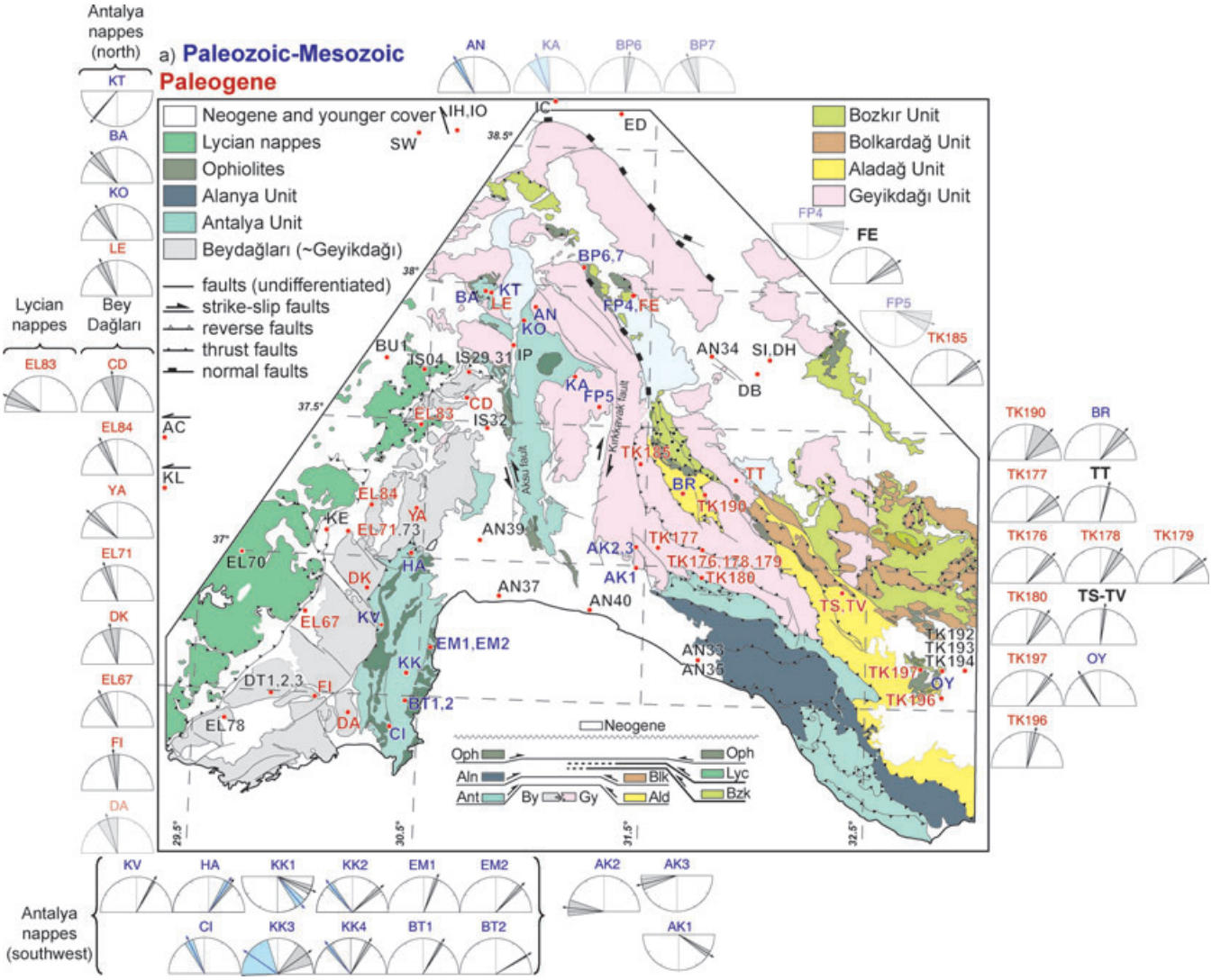


**Figure 2.** (a–c) Maps with the nappes in the research area. Locations of the sites and declinations with their corresponding $\Delta D_x$ (grey shading) from published data are indicated in for four different time intervals. (a) Palaeozoic–Mesozoic (in dark blue) and Palaeogene (in red), (b) early-middle Miocene (in dark blue) and late Miocene (in red) and (c) Pliocene–Pleistocene. Red site codes indicate the sites that are from the shown age interval. Light blue shading in declination plots indicate the *in situ* declinations for sites that are (possibly) remagnetized.

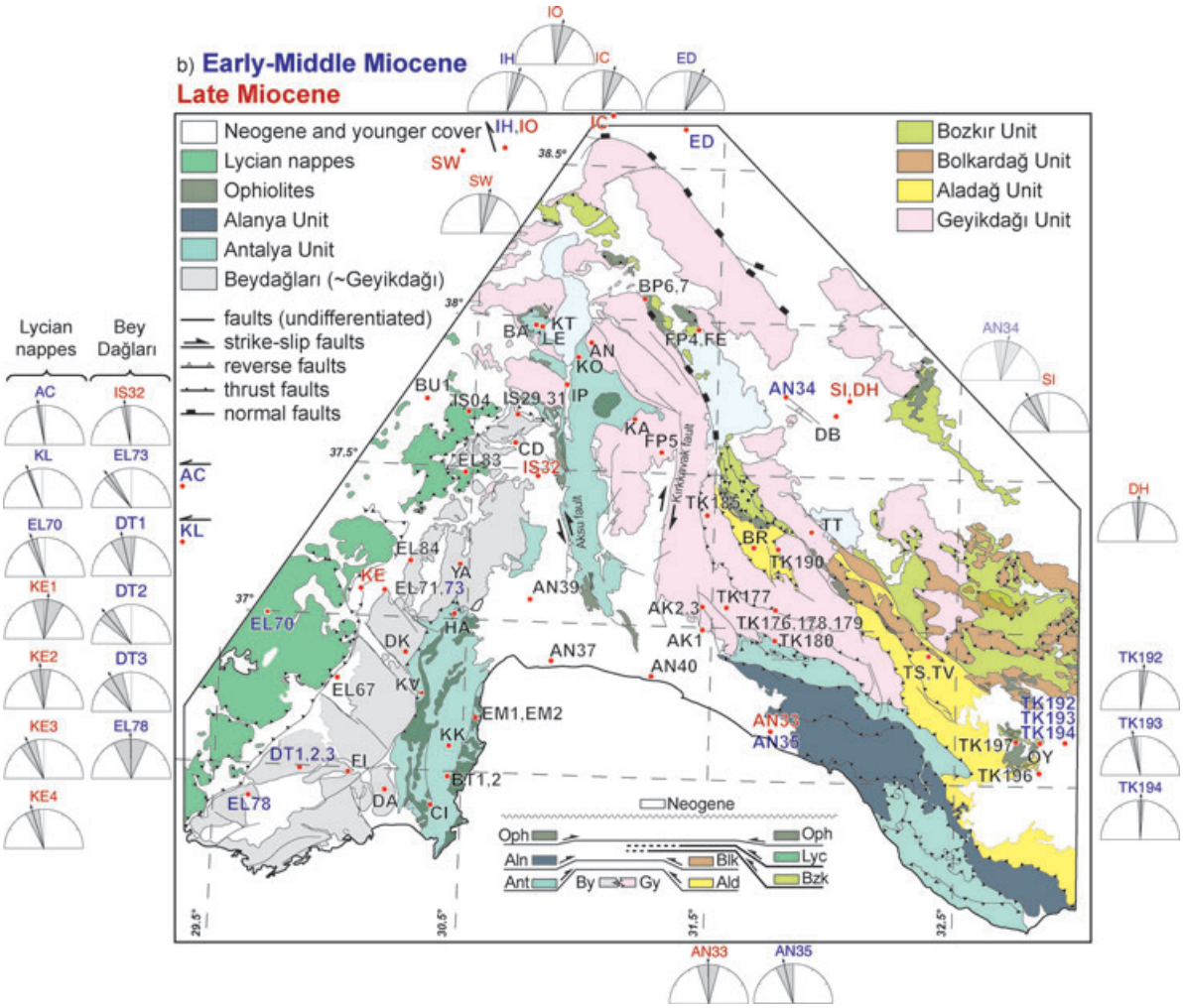


**Figure 2.** (*Continued.*)

*et al*. 1975), (2) the nappes north of Geyikdağı (Aladağ, Bolkardağ and Bozkır Nappes) originated from the north and the ones in the south (Antalya and Alanya Nappes) originated from the south (Dumont *et al*. 1972; Şengör & Yilmaz 1981) and (3) all the nappes originated from the north, except for the western part of the Antalya Nappes which is thrusted over the Beydağları Unit (Fig. 2; Ricou *et al*. 1979).

A long compressive deformation phase that resulted in nappe stacking and ophiolite obduction initiated in the late Cretaceous and continued into the early Eocene (~95–50 Ma; Okay *et al*. 2001). This resulted in the deposition of Palaeocene to middle Eocene turbidite units on top of the carbonates (Dean & Monod 1970), that mark the timing of youngest compression-related sedimentation of the ATB, contemporaneous with the collision of the ATB with the Pontides of northern Turkey (Şengör & Yilmaz 1981; Okay 1984; Tüysüz 1999; Kaymakci *et al*. 2009). Nevertheless, ophiolites and ophiolitic units share the highest structural position, and have metamorphic sole ages of ~95–90 Ma, which mark the minimum age for the onset of (intraoceanic) subduction north of the ATB (Dilek & Whitney 1997; Dilek *et al*. 1999; Yalınız *et al*. 2000; Çelik & Delaloyle 2003; Çelik *et al*. 2006; Elitok & Drüppel 2008).

After Eocene times, the Tauride fold-and-thrust belt was deformed into a peculiar, triangular bend that is known as the Isparta Angle (Fig. 1). To the west, the Taurides fold-and-thrust belt is overthrusted by the Lycian Nappes, over the Beydağları platform. The Beydağları platform is overthrusted by the Antalya Nappes from the east to southeast (Fig. 2; Robertson & Woodcock 1981; Poisson *et al*. 2003b). During the thrusting of the Lycian Nappes over the Beydağları platform in the early Miocene, a lower Miocene foreland basin was established in response to southeastward emplacement of the Lycian Nappes (Hayward 1984; Collins & Robertson 1998; Kosun *et al*. 2009; van Hinsbergen 2010; van Hinsbergen *et al*. 2010b). This was followed by a middle to latest Miocene counter-clockwise vertical axis rotation episode (Kissel & Poisson 1987; Morris & Robertson 1993) that affected the entire western limb of the Isparta Angle, including the Lycian Nappes and Beydağları region. The region was bounded in the east by transpression partitioned along the Aksu thrust and Kırkkavak strike-slip fault (Fig. 2; Kissel & Poisson 1987; Morris & Robertson 1993; van Hinsbergen *et al*. 2010a,b). This is reflected by strong folding and thrusting of the lower to uppermost Miocene stratigraphy in the Aksu and Köprüçay Basins which are bordered by these faults (Flecker *et al*. 1995; Glover & Robertson 1998; Poisson *et al*. 2003a; Çiner *et al*. 2008).

The eastern limb of the Isparta Angle (central Taurides), where we conducted our study, has a different late Cenozoic history. The late Cretaceous to Eocene compression episode formed the fold-and-thrust belt of the central Taurides, which is structurally (but

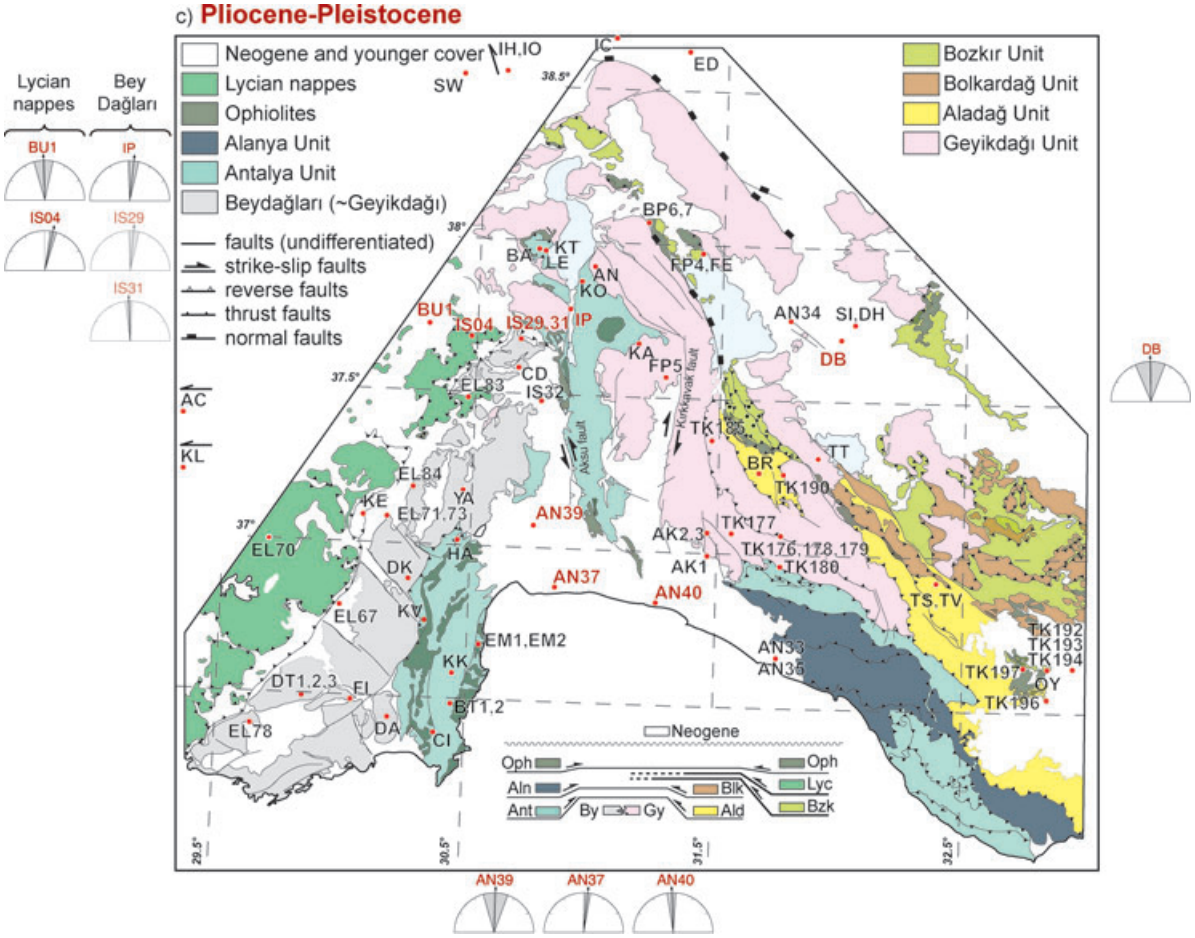


**Figure 2.** (*Continued.*)

not temporarily) equivalent to the Lycian Nappes to the west. The central Taurides fold-and-thrust belt is unconformably overlain by Miocene marine and terrestrial deposits in the Beyşehir, Manavgat, Ermenek and Mut basins, which are only very mildly deformed by normal and strike-slip faults (Bassant *et al*. 2005; Deynoux *et al*. 2005; Eris *et al*. 2005; Çiner *et al*. 2008). A palaeomagnetic study by Kissel *et al*. (1993) showed evidence for strong clockwise rotation over an angle of approximately 40° measured in Eocene rocks of the fold-and-thrust belt, whereas available data from the Miocene show no significant rotations here. Hence, they argued that the eastern limb of the Isparta Angle underwent a clockwise rotation phase sometime during the late Eocene and Oligocene, as opposed to the much younger middle Miocene rotation with opposite sense that was reconstructed for the western limb.

## 3 PALAEOMAGNETIC SAMPLING, ANALYSIS AND ROCK MAGNETIC ANALYSIS

### 3.1 Palaeomagnetic sampling

The original focus of this study was reconstructing the palaeolatitude position of the Taurides since the Carboniferous, on the basis of new palaeomagnetic data and a reappraisal of previous work. Therefore, we sampled Carboniferous to Palaeocene sections and localities in three areas within the Geyikdağı and Aladağ units in the central Taurides: Fele (north of lake Beyşehir), Seydişehir (west of Suğla lake) and Taşkent (south of Hadim; Fig. 3). All samples were taken from limestones, except site TT7 (Seydişehir section), which was sampled in siltstones and claystones.

The Seydişehir section consists of 22 sites (428 collected cores) and covers a time span from approximately middle Jurassic to Palaeocene. A stratigraphic log with assigned biostratigraphic ages of the Seydişehir section (TT1, TT2 and TT20–TT39) is given in Fig. 4 and covers a time span from middle Jurassic to Palaeocene. Several individual sites that are not part of the section (TT0 and TT3–TT7) were sampled around the lower part and above the section (159 collected cores). Those sites yield ages ranging from late Triassic to middle and possibly late Jurassic for the lower part (TT3–TT5) and Campanian-Palaeocene for the upper part (TT6–TT7). Those ages were taken from the geological map of Şenel *et al*. (2001). The lower Jurassic is absent in this region.

Near the village of Fele (Fig. 3), we sampled a section (9 sites with 200 cores) covering a time span from middle Jurassic to late Cretaceous, that was previously biostratigraphically dated (Altıner *et al*. 1999; Yılmaz & Altıner 2006). Samples were taken from nine regularly spaced sites within the section, that were correlated to the stratigraphic columns in Altıner *et al*. (1999) and Yılmaz & Altıner (2006). Samples were collected using a motor drill or an electric drill with generator. Sample orientations were measured with a compass and sample orientations as well as bedding attitudes were corrected for present-day declination (~4°W).

Around the village of Taşkent, four sites were sampled (79 cores). Site TV was sampled at the Tournaisian–Visean boundary

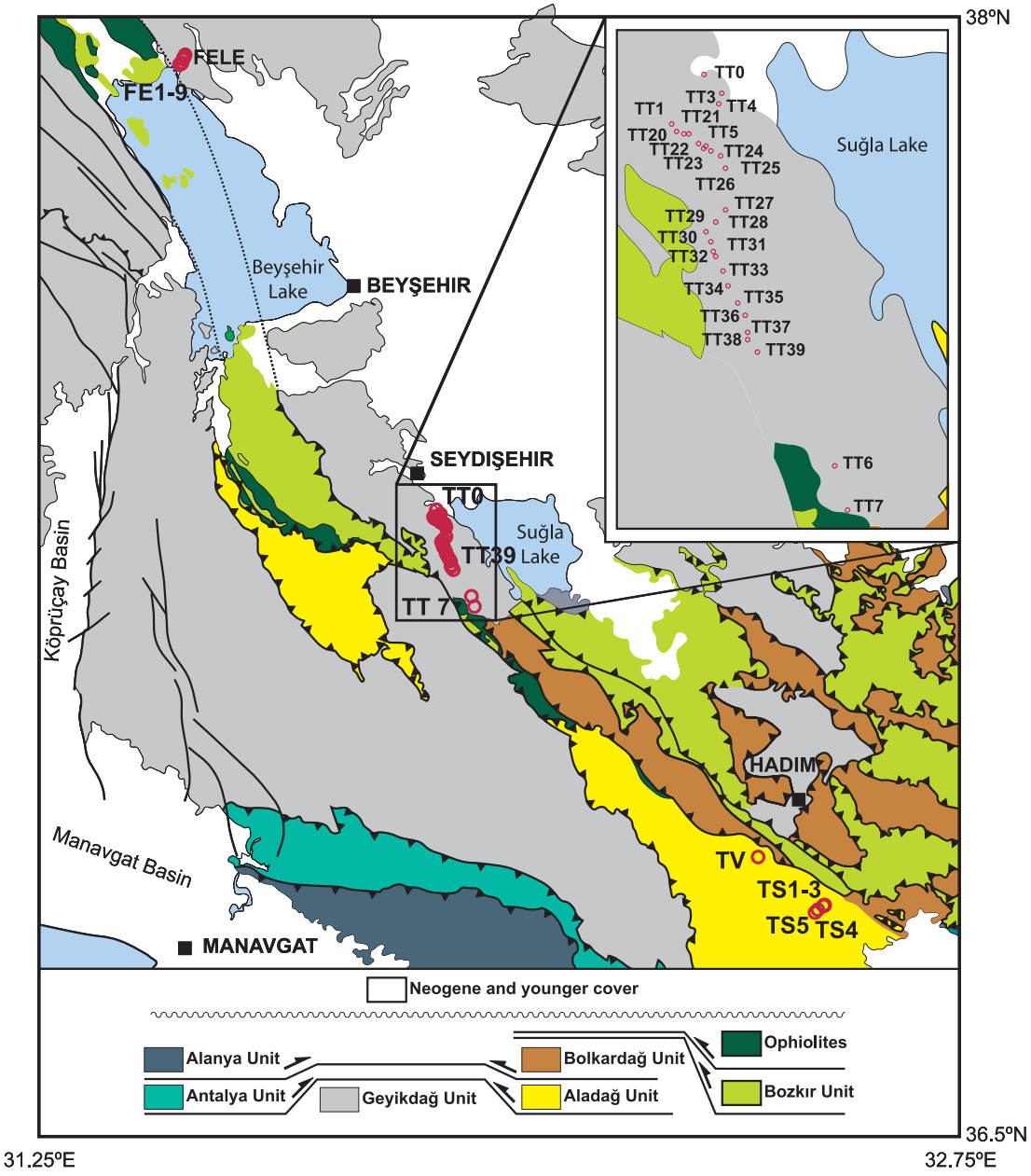


**Figure 3.** Detailed map of the study area, indicating the nappe units and the sampling sites.

(Peynircioğlu 2005). Sites TS1,2,3 were sampled in Changhsingian (upper Permian) limestones (Data S1 and Payne *et al*. 2007). Sites TS4 and TS5 were sampled in Spathian (upper Olenikian, lower Triassic) limestones (Data S1).

### 3.2 Palaeomagnetic analysis

Samples were demagnetized using alternating field (AF) and thermal (TH) progressive stepwise demagnetization methods. AF demagnetized samples were pre-heated until 150 °C prior to AF demagnetization to remove possible stress in magnetite grains caused by surface oxidation at low temperatures (LT; Van Velzen & Zijderveld 1995). Many samples however, gave erratic thermal demagnetization behaviour owing to their low natural remanent magnetization (NRM) intensity and could only be measured thermally until 150 °C. The samples were therefore mostly AF demagnetized on the inhouse developed robotized 2G DC SQUID magnetometer (noise level $10^{-12}$ Am$^2$). This procedure appeared to yield significantly better data on the low-intensity limestones (*cf.* Gong *et al*. 2008b).

Demagnetization of the NRM is displayed in orthogonal vector diagrams (Fig. 5; Zijderveld 1967). Magnetization components were determined using principal component analysis (Kirschvink 1980), typically on five to seven successive AF or temperature steps. Occasionally, a great-circle approach (McFadden & McElhinny 1988) was used when samples yielded NRM directions that were intermediate between two components with overlapping coercivity or unblocking temperature spectra (Figs 5g, h, k and l). This method determines the direction that lies closest on the great circle to the average direction from well-determined NRM

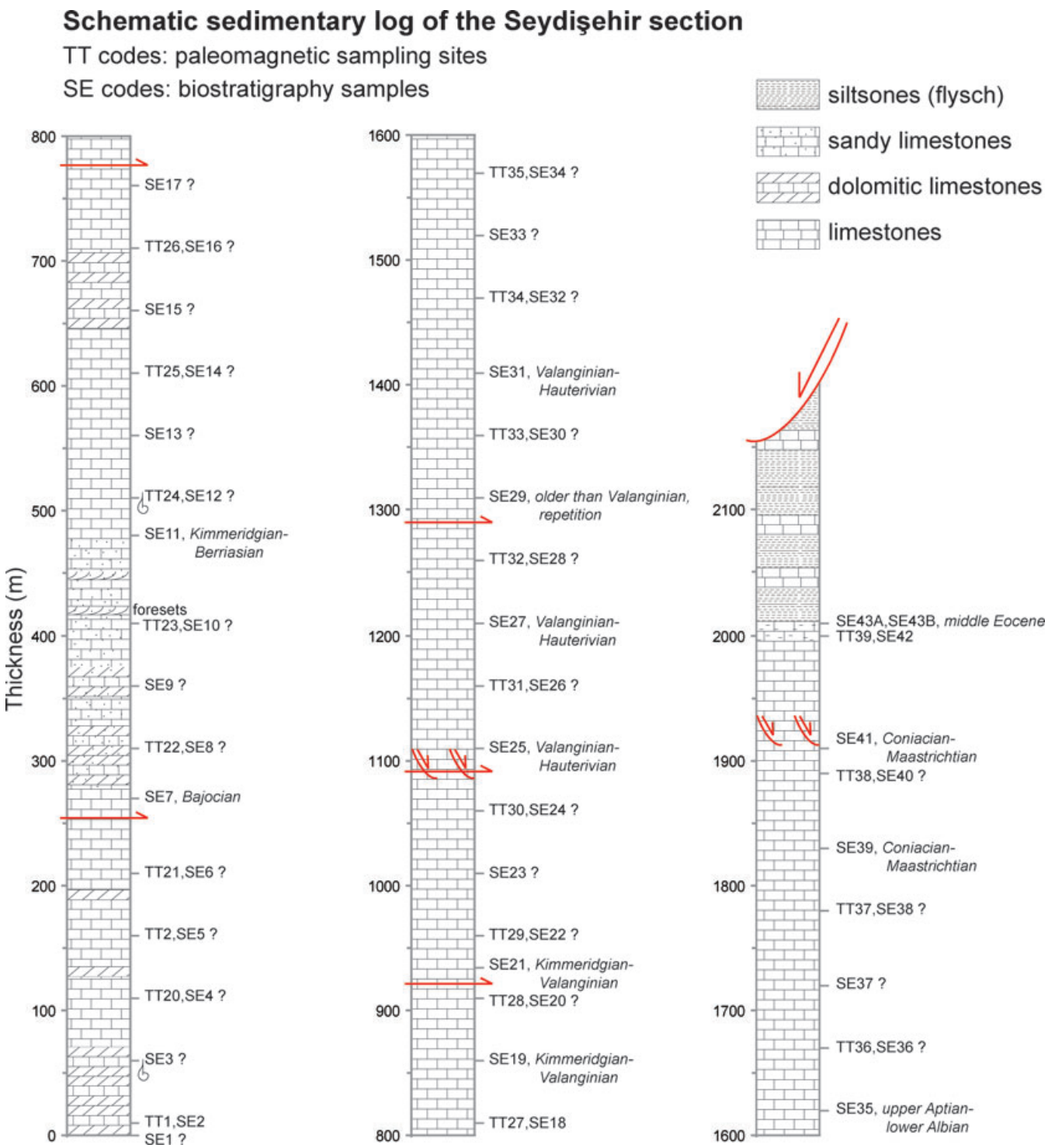


**Figure 4.** Schematic sedimentary log of the Seydişehir section. Thicknesses comes from field estimates and could therefore be an over- or underestimation of the real thickness. Red lines and arrows indicate faults.

directions. The majority of the samples, mostly limestones, have a characteristic remanent magnetization (ChRM) carried by magnetite, as is evidenced by typical maximum unblocking fields of 60–100 mT. Erratic behaviour of samples above ∼350 °C (Figs 5d and j), also indicates the presence of iron sulfides.

Site mean directions as well as virtual geomagnetic poles (VGP) and their means were calculated from the ChRM directions (Fisher 1953). Per site, a variable cut-off (Vandamme 1994) was applied on the VGPs. The sample directions that were rejected on the basis of this cut-off are indicated in Fig. 6. We calculated the error in declination ($\Delta D_x$) and the error in inclination ($\Delta I_x$) following Butler (1992). This approach is favoured because it more realistically describes the directional distributions that become increasingly elongated with lower latitudes (Creer *et al*. 1959; Tauxe & Kent 2004;

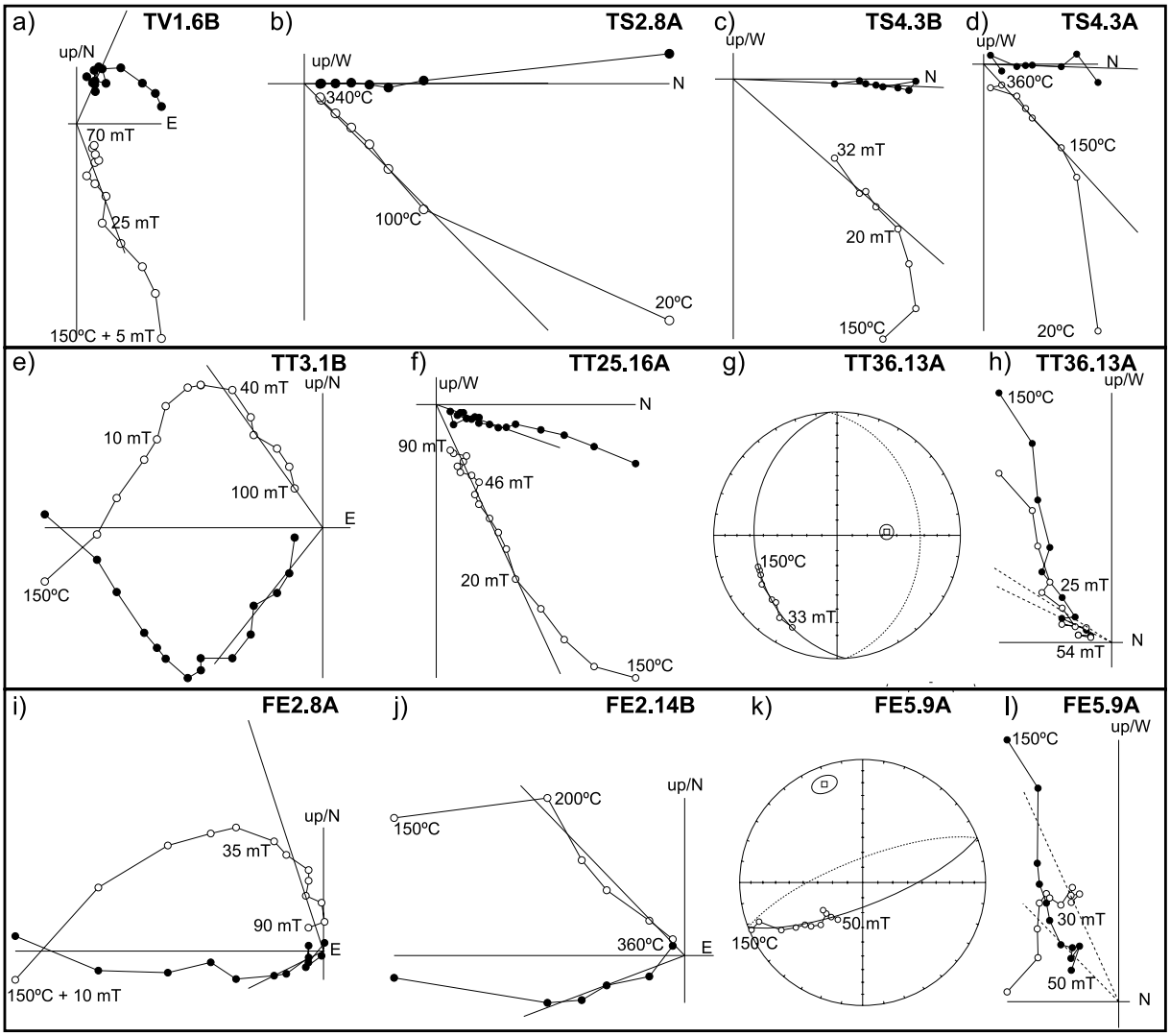


**Figure 5.** Orthogonal vector diagrams (Zijderveld 1967), showing characteristic demagnetization diagrams for representative sampled sites. Closed (open) circles indicate the projection on the horizontal (vertical) plane. Alternating field and thermal demagnetization steps are indicated. All diagrams are displayed after bedding tilt correction.

Tauxe *et al*. 2008). For all previously published data we calculated the $A_{95}$ from the $\alpha_{95}$, usually given in literature, using the Creer transformation (Creer 1962).

On the data of the Seydişehir section, we applied the fold test of Tauxe & Watson (1994) and the small circle intersection (SCI) method of Shipunov (1997) to determine the percentage of unfolding at which the remagnetization magnetization was acquired. The SCI method was proposed by Shipunov (1997) and later modified by Waldhör & Appel (2006). It is especially useful for synfolding remanences. The method estimates the paleomagnetic direction at the moment of remagnetization from a group of sites, using the variability in bedding strike of tilted sediments. The SCI method is geometrically alternative to the classical fold tests, as the resulting field direction does not depend on the final amount of tilting the remanences underwent. The former assumption of a proportional way of tilting is not needed. We chose to apply these tests on the Seydişehir section, because of the large amount of data that is available. Sites TT7 and TT28 were excluded from analysis, because of the low number of individual directions ($N = 2$).

### 3.3 Supporting rock magnetic analyses

#### *3.3.1 Acquisition curves of the isothermal remanent magnetization*

The palaeomagnetic data obtained from this study are most probably subject to remagnetization. Therefore, isothermal remanent magnetization (IRM) curves were acquired, to complement the palaeomagnetic analysis and to further characterize the rock magnetic behaviour of the samples. We carried out the IRM measurements on 174 specimens from the Seydişehir section, because we intended to run end-member modelling on this section (Weltje 1997; Heslop & Dillon 2007; Heslop *et al*. 2007; Gong *et al*. 2009a), that may indicate remagnetization of the rocks. The Seydişehir section consists of many levels and rock types (limestones, sandy/shaly limestones, dolomitic limestones), compared to the Fele and Taşkent localities, and therefore had our preference. Before IRM acquisition, the specimens were pre-heated until 150 °C in a magnetically shielded oven and subsequently all specimens were AF demagnetized at 300 mT in three orthogonal directions, to minimize the influence of

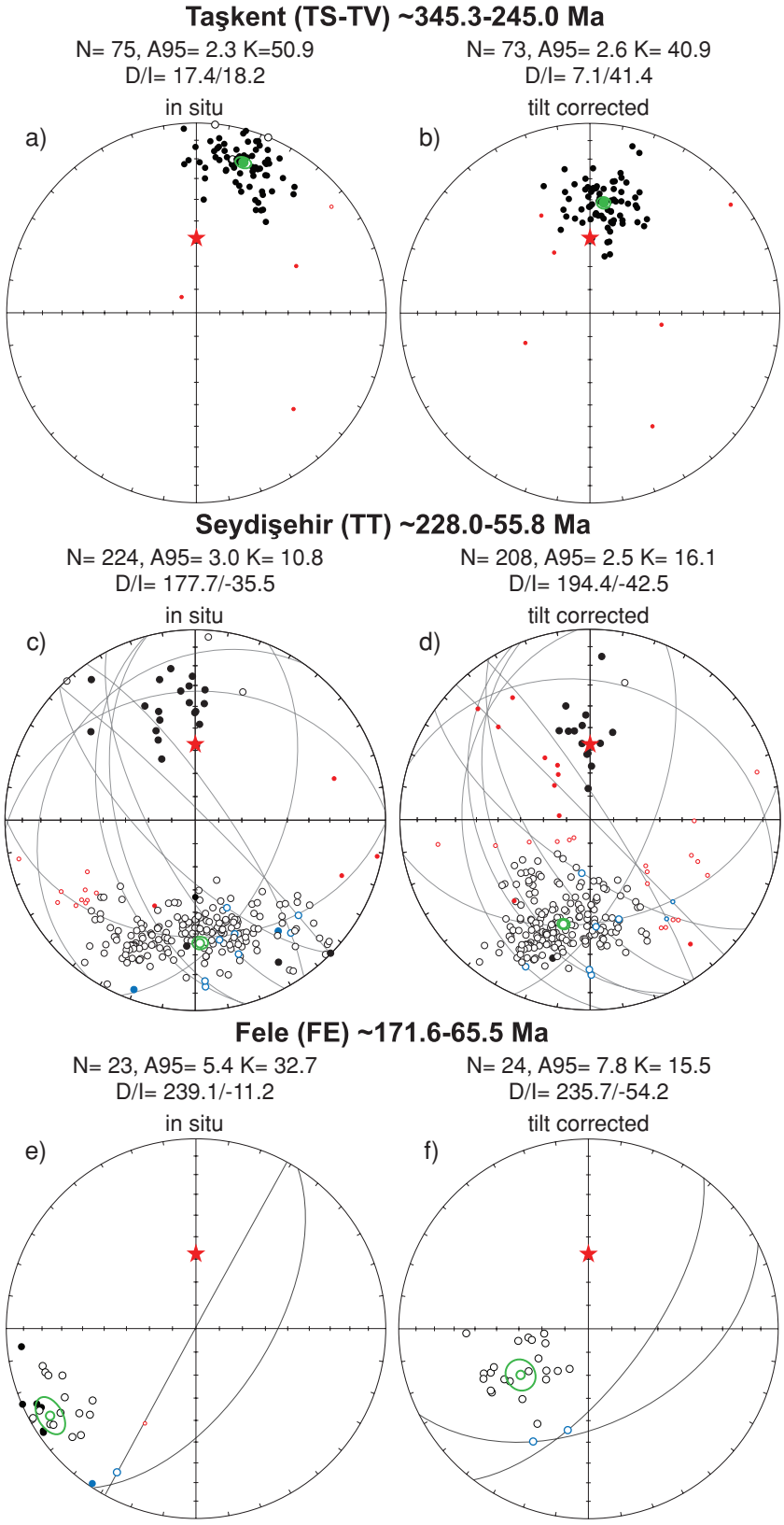


**Figure 6.** Equal area projections of the ChRM directions of all sections (Table 1). Open (closed) symbols denote projection on upper (lower) hemisphere. Large green circles with green circle indicate respectively the mean directions and their cone of confidence ($\alpha_{95}$) after (right-hand side diagrams) and before tilt correction (left-hand side diagrams). Red (small) circles indicate the individual directions rejected by the Vandamme cut-off angle (Vandamme 1994). Black lines indicate the great circles that were used to calculate the best fitting ChRM directions, with the corresponding calculated directions in blue (McFadden & McElhinny 1988). Red asterisks indicates the present-day geocentric axial dipole direction at the sampled location.

magnetic interaction and thermal activation on the shape of the IRM acquisition curves and to guarantee an IRM curve shape as close as possible to a cumulative log-Gaussian distribution (Heslop *et al*. 2004). As with the AF demagnetization of the NRM, the preheating at 150 °C was done to remove or reduce the influence of potentially present oxidized surface layers around fine-particle magnetite (*cf.* Van Velzen & Zijderveld 1995). The IRM was acquired in 57 steps up to 700 mT, with the in-house developed robotized magnetometer. IRM component analysis to identify the different IRM components was done according to Kruiver *et al*. (2001). In this approach, IRM components are considered cumulative log-Gaussian distributions that are characterized by their saturation isothermal remanent magnetization (SIRM), the peak field at which half of the SIRM is reached ($B_{1/2}$), and the dispersion or width of the corresponding distribution (DP, Kruiver *et al*. 2001). In practice, many IRM acquisition curves are not entirely cumulative log-Gaussian as a consequence of potentially present magnetic interaction (although in these weakly magnetic sediments it is anticipated to be marginal) and thermal activation characteristic of small magnetic particles (Egli 2004; Heslop *et al*. 2004). The IRM acquisition curves could be interpreted with either two or three magnetic components, overlapping in coercivity spectrum. Usually, a low intensity and low coercivity component is observed, a result of slightly skewed-to-the-left data (Heslop *et al*. 2004). This component is not assigned a physical meaning, because it is a consequence of the method only being able to fit symmetric distributions; its contribution is added to the low-coercivity component.

### *3.3.2 End-member modelling of the IRM acquisition curves*

In a number of cases remagnetization shows up by means of specific magnetic properties. For example, the so-called 'remagnetized' and 'non-remagnetized' trends based on hysteresis parameters are documented for limestones (e.g. Channell & McCabe 1994). However, many data sets of remagnetized rocks plot in between the two trend-lines, which makes the interpretation rather equivocal (e.g. Katz *et al*. 2000; Zegers *et al*. 2003). In addition, it is technically not straightforward to measure meaningful hysteresis parameters in weakly magnetic rocks like those in the present investigation. To circumvent these problematic aspects, Gong *et al*. (2009a) proposed to perform end-member modelling on IRM acquisition curves to diagnose remagnetization independent of palaeomagnetic directional information. A chemically precipitated suite of magnetic particles as a consequence of burial is expected to have magnetic properties subtly different from a detrital magnetic particle ensemble. The diagenetically precipitated magnetite can be formed in the presence of internally buffered or by means of externally derived fluids. The latter is considered less likely because in the study area no evidence was found, like low-temperature so-called 'Mississippi Valley Type' ores. IRM acquisition curves determined with a large number of field steps can visualize such small differences. In a study on Cretaceous limestones from the Pyrenees, Gong *et al*. (2009a) discriminated remagnetized and non-remagnetized limestones with a high level of statistical significance ($\gg$95 per cent). van Hinsbergen *et al*. (2010b) used a similar approach to show that Miocene limestones from the Beydağları platform (western Turkey) that were overthrusted by the Lycian Nappes are not remagnetized and likely carry a primary NRM.

End-member modelling is a non-parametric inverse technique, meaning that the model is determined from the data. By iterative minimization the data variability is described by a linear combination of a number of invariant points, termed end-members. Both the shape as well as the number of end-members is determined by so-called bilinear unmixing, which makes the method powerful. Simultaneously, it has potential pitfalls: since (almost) everything is possible, the user must have at least a certain idea about the significance of potential end-members: the solution is mathematically non-unique and the most reasonable geological solution should be targeted (*cf.* Weltje 1997). It must be reasonably certain that the entire data variability has been sampled; otherwise the resulting end-members are not representative. We therefore determined IRM acquisition curves for the limestones, dolomitic limestones, sandy limestones and shaly limestones of the Seydişehir section. After this the data groups were merged and essentially the same end-members were calculated. This implies that the entire data variability was sampled and that the outcome of the analysis is not input-dependent (as would have been the case if the total data variability would not have been sampled). For all end-member calculations, the bilinear-unmixing algorithm of Weltje (1997) programmed by D. Heslop in MATLAB was utilized. This algorithm determines the minimum hull around the data space, which ensures geologically most interpretable end-members (Weltje 1997). It starts with a configuration within the data cloud, which is iteratively enlarged by moving the end-member compositions minimally, ideally until all data points are included. In practice, it is accepted that some data points remain outside the calculated hull, which makes the algorithm less sensitive to outliers, a distinct advantage over other bilinear-unmixing approaches. The algorithm dictates that input curves should be monotonously increasing (Weltje 1997; Heslop & Dillon 2007). All IRM curves will be normalized to their maximum value, thus forming a closed data set. Therefore, the abundances of the various end-members will not be independent, that is, changes in the abundance of an end-member will affect the abundances of other end-members. The programme performs a maximum of 1000 iterations, unless the maximum convexity level of –6 (a descriptor of the distance between the data outside the hull and the calculated minimum hull) is reached earlier. The convexity level at termination is used as a judgment on the quality of the model for the particular data set.

As mentioned earlier on, the signatures of the individual end-members must be understood for an optimal analysis. It is likely that end-members should be interpreted along the lines of magnetic minerals. Therefore, we plotted all IRM acquisition curves and analysed 21 IRM acquisition curves (one from each site) using the cumulative log-Gaussian approach of Kruiver *et al*. (2001). This is a parametric approach to identify the different coercivity components, which serves as a guideline for the interpretation of the end-members. The estimation of the number of meaningful end-members is based on the calculation of the coefficient of determination ($r^2$, ranging from 0 to 1) between the input data and the end-member models (Heslop & Dillon 2007), that are calculated by the programme for two through nine end-members. A low $r^2$ ($r^2 <$ 0.5) will reflect a non-adequate description of the variance of the input data set. Ideally, the $r^2$ value is high ($>$0.8) and addition of extra end-members will provide only small increase in $r^2$. When the $r^2$ values are plotted versus the corresponding end-member number, the optimum number of end-members would correspond to the break-in-slope, equivalent to the 'scree-test' regularly used in exploration geology. The shape of the end-members should be sufficiently different to avoid over-interpretation of end-members. To ensure monotonously increasing IRM acquisition curves, IRM data were used starting at 8 mT fields. Inspection of the data revealed

that the data from lower (pulse) fields were fairly noisy because of very low IRM increments.

## 4 PALAEOMAGNETIC AND ROCK MAGNETIC RESULTS

### 4.1 Palaeomagnetic results—demagnetization of the NRM

#### *4.1.1 Taşkent*

The samples of sites TV and TS1–3 have initial intensities of ∼350–3000 $\mu$A m$^{-1}$, those of TS4 and TS5 are lower, ∼130–600 $\mu$A m$^{-1}$. In the majority of the samples, a LT or low coercive force (LC) component is present until ∼200 °C or ∼150 °C plus ∼25 mT. The ChRM direction was usually isolated between ∼200 °C and 360 °C or between ∼25 mT and 90 mT in 79 samples (Fig. 5). All sites around Taşkent yield very similar palaeomagnetic directions (Table 1, Figs 6 and 9), which is unlikely for the long time interval between early Carboniferous and late Permian/early Triassic. Furthermore, all samples show normal polarities, even though they were deposited in a period of dominantly reversed polarity (Davydov *et al*. 2004; Wardlaw *et al*. 2004), including the Permo-Carboniferous Reversed Superchron (PCRS). We therefore conclude that the Taşkent sites must have been remagnetized at any time after the early Triassic.

#### *4.1.2 Seydişehir*

From the Seydişehir section, 28 sites were sampled (TT0–7 and TT20–TT39), with ages ranging from late Triassic to Palaeocene (Fig. 4). Ages were assigned to the sites on the basis of biostratigraphy, (Data S1 and Table 1). The limestone samples yield initial intensities of ∼100–2000 $\mu$A m$^{-1}$, whereas intensities after pre-heating until 150 °C range from ∼5–300 $\mu$A m$^{-1}$. The silt/claystone samples from site TT7 yield higher intensities after pre-heating of ∼450–700 $\mu$A m$^{-1}$. An LC component up to ∼30 mT is present in the lowest part of the section (sites TT0–TT3), which resembles the present-day geocentric axial dipole (GAD) direction. The high coercivity (HC) component, interpreted to be the ChRM component, was isolated between ∼30 mT and 90 mT in 231 samples (Table 1, Fig. 5). For 10 other samples, we used the remagnetization great-circle approach (Figs 5g and k). Most samples yielded reversed polarities (90 per cent). The majority of the sites yielded a reversed polarity, some sites yielded normal polarities, while in some sites both normal and reversed polarities were detected. The directions are clearly shallower than the GAD direction before tilt correction (Fig. 6c). We note that site TT36, which is taken from an Albian interval, yielded reversed polarities, in an interval that is part of the Cretaceous Normal Superchron (CNS). Moreover, all sites yielded very similar palaeolatitudes around 30°N (Table 1, Fig. 6) despite age differences of up to ∼200 Myr. Again, we must suspect that all rocks in the Seydişehir section are remagnetized. It is important to note here that the Palaeocene site TT7 (that is significantly younger than the rest of the sites) is based on only two data points. Although the palaeomagnetic directions obtained from site TT7 are similar to the data from the entire Seydişehir section, we will not include this site in the discussions. Conclusions on the age of remagnetization based on this site would be speculative.

After applying the fold test and the SCI method on all data (excluding TT7 and TT28), we decided to exclude also sites TT0, TT3 and TT32, because of their deviation from other sites when applying the SCI method (Data S2e). Moreover, the fold test and SCI method show much better agreement after omitting these three sites. Deviation of site TT3 from the other sites is most likely caused by the presence of a strike-slip fault that probably caused rotation of the site. For sites TT0 and TT32 we did not find direct evidence for relative rotation, and data from the two sites are most probably statistically deviating. The results of the fold test and the SCI method can be found in Data S2. Both methods suggest a syn-folding magnetization that was acquired at ∼65–68 per cent untilting, so during the early stages of folding. The fold test suggests remagnetization at a direction of $D = 176.2°$, $I = –43.6°$, the SCI method at $D = 183.8°$, $I = -44.7°$, so at an average latitude of ∼26°N.

#### *4.1.3 Fele*

From the middle Jurassic to upper Cretaceous of the Fele section, nine sites (FE1–FE9) were sampled. Intensities (after pre-heating) typically range ∼20–550 $\mu$A m$^{-1}$. Intensities of FE8 and FE9 showed even lower intensities, ranging 20–50 $\mu$A m$^{-1}$. For this reason, these two sites revealed no interpretable results. A characteristic component was isolated generally between ∼35/40 mT and 90 mT (Figs 5i–l) in 22 samples. For two other samples, we made use of the great-circle approach (Fig. 5k). Rocks from all sites, recorded a reversed magnetic polarity (Table 1, Figs 6e and f), including site FE7 which has a Cenomanian age. Importantly, the Cenomanian is a stage entirely within the CNS (Ogg *et al*. 2004). A solely reversed ChRM direction in rocks ranging in age from Bajocian–Maastrichtian, including rocks deposited during the CNS, implies that also this entire section was subject to remagnetization.

### 4.2 Rock magnetic results

#### *4.2.1 Acquisition curves of the IRM*

First, we will describe the analysis of the IRM acquisition curves using the log-Gaussian approach of Kruiver *et al*. (2001). Results are compiled in Fig. 7 and Table 2. The diagrams show three components: a magnetite component with a $B_{1/2}$ ranging ∼50–60 mT and a relatively large DP, a HC mineral and in some cases a very low coercivity component. The HC mineral can be either hematite or goethite, but because the rocks have probably been buried relatively deeply, we consider this a hematite component since goethite is thermodynamically not stable anymore above temperatures as low as c. 100 °C under geological conditions (Langmuir 1971). Yapp (1983) calculated that substitution of aluminium for iron stabilizes the goethite structure, but for goethite to persist under the estimated conditions (c. 150–200 °C) that prevailed during nappe stacking a substantial level of substitution is required which easily would result in Néel temperatures below room temperature. The magnetite component is most dominantly present in (partly) dolomitized rocks and in the upper part of the section in site TT39, where the limestones contain some silt. The hematite component is generally present in non-dolomitic and non-sandy intervals. The third component (without physical meaning) is not always clearly visible, owing to the fairly large DP of the magnetite component. This is interpreted to be caused by a rather broad grain size distribution, that is, resulting from chemical remagnetization where a second generation of small magnetite particles is formed. End-member modelling can visualize potentially small differences amongst the samples and these can be

**Table 1.** Table showing all data from this study.

| | | | | | | | ChRM directions—*in situ* | | | | | | | | | | | | ChRM directions—tilt corrected | | | | | | | | | | | |
|---|---|---|---|---|---|---|---|---|---|---|---|---|---|---|---|---|---|---|---|---|---|---|---|---|---|---|---|---|---|---|
| | Epoch/Stage | Age (Ma) | Age error (Ma) | Lat | Long | *N*c | *N*/*N*a | *D* | *I* | Δ*D*x | Δ*I*x | λ | *k* | $\alpha_{95}$ | *K* | $A_{95}$ | $\Delta\lambda^+$ | $\Delta\lambda^-$ | Strike/dip | *N*/*N*a | *D* | *I* | Δ*D*x | Δ*I*x | λ | *k* | $\alpha_{95}$ | *K* | $A_{95}$ | $\Delta\lambda^+$ | $\Delta\lambda^-$ |
| Seydişehir | | | | | | | | | | | | | | | | | | | | | | | | | | | | | | | |
| TT0 | Late Triassic? | 213.8 | 14.2 | 37.381 | 31.865 | 25 | 19/27 | 230.6 | −31.7 | 4.0 | 6.1 | 17.2 | 64.5 | 4.2 | 78.2 | 3.8 | 4.0 | 3.7 | 163/23 | 19/27 | 221.0 | −50.6 | 5.5 | 5.2 | 31.3 | 66.8 | 4.1 | 51.8 | 4.7 | 4.9 | 4.5 |
| TT1 | Middle Jurassic? | 168.4 | 7.2 | 37.372 | 31.860 | 20 | 13/14 | 157.9 | −33.3 | 4.4 | 6.5 | 18.2 | 85.8 | 4.5 | 99.0 | 4.2 | 4.4 | 4.0 | 016/21 | 13/14 | 172.3 | −44.1 | 5.2 | 5.9 | 25.9 | 85.7 | 4.5 | 80.2 | 4.7 | 5.0 | 4.3 |
| TT2 | Middle Jurassic? | 168.4 | 7.2 | 37.369 | 31.865 | 8 | 8/8 | 190.0 | −35.1 | 5.9 | 8.3 | 19.4 | 74.5 | 6.5 | 100.7 | 5.5 | 5.9 | 5.2 | 022/14 | 8/8 | 200.0 | −36.7 | 6.5 | 9.0 | 20.4 | 74.6 | 6.5 | 82.5 | 6.1 | 6.7 | 5.7 |
| TT3 | Middle Jurassic? | 168.4 | 7.2 | 37.373 | 31.870 | 31 | 49/50 | 204.8 | −28.0 | 2.1 | 3.3 | 14.9 | 74.6 | 2.4 | 104.1 | 2.0 | 2.0 | 1.9 | 066/14 | 49/50 | 212.0 | −36.7 | 2.2 | 3.0 | 20.4 | 74.8 | 2.4 | 97.8 | 2.1 | 2.1 | 2.0 |
| TT4 | Middle Jurassic? | 168.4 | 7.2 | 37.372 | 31.870 | 11 | 16/16 | 136.2 | −18.1 | 9.4 | 17.2 | 9.3 | 9.6 | 12.6 | 16.7 | 9.3 | 10.2 | 8.8 | 027/58 | 16/16 | 172.2 | −68.6 | 34.0 | 14.2 | 51.9 | 8.4 | 13.5 | 4.3 | 20.2 | 23.9 | 17.0 |
| TT5 | Middle–late Jurassic? | 160.55 | 15.05 | 37.366 | 31.873 | 30 | 6/14 | 151.0 | −34.6 | 18.9 | 27.0 | 19.0 | 13.1 | 19.2 | 15.1 | 17.8 | 23.7 | 15.2 | 003/26 | 6/14 | 171.2 | −44.4 | 26.4 | 29.8 | 26.1 | 10.7 | 21.4 | 9.1 | 23.5 | 34.4 | 18.7 |
| TT6 | Cenomanian(-Campanian?) | 96.6 | 3.1 | 37.263 | 31.920 | 43 | | | | | | | | | | | | | | | | | | | | | | | | | |
| TT7 | Paleocene | 60.65 | 4.85 | 37.245 | 31.923 | 19 | 2/4 | 320.6 | 40.9 | - | - | 23.4 | - | - | - | - | - | - | 333/09 | 2/4 | 328.5 | 42.2 | - | - | 24.4 | - | - | - | - | - | - |
| TT20 | Post-Liassic–pre-Bajocian | 173.6 | 2 | 37.370 | 31.862 | 20 | 16/18 | 168.1 | −37.9 | 5.3 | 7.0 | 21.3 | 49.3 | 5.3 | 57.7 | 4.9 | 5.2 | 4.6 | 034/19 | 15/18 | 183.8 | −48.5 | 7.1 | 7.2 | 29.5 | 44.6 | 5.8 | 39.1 | 6.2 | 6.7 | 5.8 |
| TT21 | Bajocian | 169.65 | 1.95 | 37.369 | 31.867 | 20 | 18/18 | 177.5 | −44.4 | 3.3 | 3.7 | 26.1 | 168.6 | 2.7 | 137.4 | 3.0 | 3.0 | 2.8 | 356/19 | 18/18 | 196.8 | −39.8 | 2.9 | 3.7 | 22.6 | 168.5 | 2.7 | 165.8 | 2.7 | 2.8 | 2.6 |
| TT22 | Bajocian–Callovian | 166.6 | 5.4 | 37.366 | 31.871 | 20 | 12/17 | 151.0 | −36.0 | 8.2 | 11.4 | 20.0 | 31.7 | 7.8 | 32.6 | 7.7 | 8.6 | 7.1 | 350/20 | 12/17 | 166.8 | −39.9 | 9.5 | 12.1 | 22.7 | 31.6 | 7.8 | 25.5 | 8.8 | 9.9 | 7.9 |
| TT23 | Bathonian–Berriasian ? | 153.95 | 13.75 | 37.364 | 31.872 | 20 | 17/18 | 171.2 | −42.5 | 4.6 | 5.5 | 24.6 | 89.0 | 3.8 | 73.2 | 4.2 | 4.4 | 4.0 | 015/21 | 17/18 | 192.8 | −47.3 | 5.1 | 5.3 | 28.5 | 89.0 | 3.8 | 65.0 | 4.5 | 4.7 | 4.3 |
| TT24 | Kimmeridgian–Berriasian | 147.95 | 7.75 | 37.364 | 31.875 | 20 | 3/8 | 175.7 | −34.2 | 52.5 | 74.2 | 18.8 | 6.2 | 54.4 | 7.5 | 48.7 | −75.1 | 41.5 | 020/30 | 3/8 | 198.9 | −40.7 | 77.5 | 86.9 | 23.3 | 6.2 | 54.5 | 4.8 | 63.8 | 56.3 | 50.8 |
| TT25 | Kimmeridgian-Valanginian | 146.05 | 9.65 | 37.362 | 31.879 | 20 | 12/18 | 160.6 | −29.3 | 11.6 | 18.3 | 15.7 | 10.0 | 14.4 | 16.0 | 11.2 | 13.0 | 10.1 | 029/12 | 12/18 | 166.3 | −37.8 | 13.5 | 18.0 | 21.2 | 10.0 | 14.4 | 12.9 | 12.5 | 15.1 | 11.0 |
| TT26 | Kimmeridgian–Valanginian | 146.05 | 9.65 | 37.359 | 31.881 | 20 | | | | | | | | | | | | | | | | | | | | | | | | | |
| TT27 | Kimmeridgian–Valanginian | 146.05 | 9.65 | 37.346 | 31.880 | 20 | | | | | | | | | | | | | | | | | | | | | | | | | |
| TT28 | Kimmeridgian–Valanginian | 146.05 | 9.65 | 37.342 | 31.877 | 20 | 2/10 | 175.1 | −36.9 | - | - | 20.6 | - | - | - | - | - | - | 114/02 | 2/10 | 174.4 | −38.7 | - | - | 21.8 | - | - | - | - | - | - |
| TT29 | Kimmeridgian–Valanginian | 146.05 | 9.65 | 37.339 | 31.873 | 20 | | | | | | | | | | | | | | | | | | | | | | | | | |
| TT30 | Kimmeridgian–Hauterivian | 142.85 | 12.85 | 37.335 | 31.875 | 19 | | | | | | | | | | | | | | | | | | | | | | | | | |
| TT31 | Valanginian–Hauterivian | 135.1 | 5.1 | 37.332 | 31.876 | 22 | 10/22 | 358.4 | 33.6 | 7.4 | 10.8 | 18.4 | 21.9 | 7.0 | 48.1 | 7.0 | 7.7 | 6.5 | 094/19 | 10/22 | 356.2 | 52.5 | 11.8 | 10.4 | 33.1 | 22.0 | 10.5 | 24.8 | 9.9 | 11.2 | 8.8 |
| TT32 | Valanginian–Hauterivian | 135.1 | 5.1 | 37.331 | 31.877 | 20 | 8/10 | 339.1 | 36.1 | 12.9 | 17.9 | 20.0 | 14.9 | 14.8 | 21.9 | 12.1 | 14.5 | 10.7 | 088/25 | 8/10 | 327.4 | 58.9 | 22.0 | 15.1 | 39.7 | 14.9 | 14.8 | 11.9 | 16.8 | 20.5 | 14.1 |
| TT33 | Valanginian–Hauterivian | 135.1 | 5.1 | 37.327 | 31.879 | 21 | | | | | | | | | | | | | | | | | | | | | | | | | |
| TT34 | Valanginian–Barremian ? | 132.6 | 7.6 | 37.322 | 31.881 | 20 | | | | | | | | | | | | | | | | | | | | | | | | | |
| TT35 | Barremian–Aptian | 121 | 9 | 37.316 | 31.885 | 20 | 9/18 | 175.4 | −41.2 | 13.4 | 16.5 | 23.6 | 20.7 | 11.6 | 18.6 | 12.3 | 14.7 | 10.7 | 038/24 | 9/18 | 198.4 | −54.0 | 18.4 | 15.3 | 34.5 | 20.7 | 11.6 | 12.7 | 15.0 | 18.3 | 12.8 |
| TT36 | Albian | 106 | 6.4 | 37.312 | 31.888 | 19 | 6/17 | 186.9 | −24.5 | 18.0 | 30.5 | 12.8 | 9.3 | 23.2 | 15.6 | 17.5 | 22.7 | 15.8 | 122/24 | 6/17 | 180.2 | −45.8 | 30.1 | 32.6 | 27.2 | 8.0 | 25.3 | 7.3 | 26.5 | 40.5 | 20.5 |
| TT37 | Cenomanian–Turonian ? | 97.65 | 8.35 | 37.307 | 31.888 | 19 | | | | | | | | | | | | | | | | | | | | | | | | | |
| TT38 | Coniacian–Maastrichtian | 77.4 | 11.9 | 37.305 | 31.889 | 20 | | | | | | | | | | | | | | | | | | | | | | | | | |
| TT39 | Middle Eocene | 44.5 | 4.1 | 37.301 | 31.892 | 20 | | | | | | | | | | | | | | | | | | | | | | | | | |
| TT all specimens | Carnian–middle Eocene | 141.9 | 86.1 | 37.362 | 31.879 | 587 | 224/285 | 177.8 | −35.6 | 3.2 | 4.5 | 19.7 | 10.6 | 3.0 | 10.8 | 3.0 | 3.1 | 2.9 | 028/21 | 208/285 | 194.4 | −42.5 | 2.8 | 3.3 | 24.6 | 17.1 | 2.4 | 16.1 | 2.5 | 2.6 | 2.4 |
| TT site average | Carnian–middle Eocene | 141.9 | 86.1 | 37.362 | 31.879 | 587 | 16/18 | 172.9 | −35.2 | 10.9 | 15.2 | 19.4 | 16.5 | 9.3 | 14.0 | 10.2 | 11.7 | 9.1 | 028/21 | 208/285 | 185.7 | −48.1 | 9.8 | 10.0 | 29.1 | 27.7 | 7.1 | 19.4 | 8.6 | 9.6 | 7.7 |
| Taşkent | | | | | | | | | | | | | | | | | | | | | | | | | | | | | | | |
| TV | Tournaisian/Visean boundary | 345.3 | 0 | 36.916 | 32.400 | 44 | 11/17 | 21.1 | 15.3 | 5.5 | 10.3 | 7.8 | 44.9 | 6.9 | 71.3 | 5.4 | 5.7 | 5.3 | 126/31 | 11/17 | 14.9 | 44.7 | 7.4 | 8.4 | 26.3 | 49.9 | 6.5 | 47.8 | 6.9 | 7.4 | 6.1 |
| TS1,2,3 | Changhsingian | 252.4 | 1.4 | 36.845 | 32.503 | 30 | 23/24 | 24.8 | 25.5 | 3.6 | 6.0 | 13.4 | 56.7 | 4.1 | 75.8 | 3.5 | 3.6 | 3.4 | 157/25 | 23/24 | 12.1 | 42.9 | 4.8 | 5.6 | 24.9 | 43.0 | 4.7 | 50.1 | 4.3 | 4.6 | 4.0 |
| TS4 | Spathian (upper Olenekian) | 248 | 3 | 36.839 | 32.491 | 49 | 27/28 | 11.1 | 14.9 | 3.5 | 6.7 | 7.6 | 33.8 | 4.8 | 63.7 | 3.5 | 3.6 | 3.5 | 133/32 | 27/28 | 359.7 | 41.5 | 5.3 | 6.5 | 23.9 | 32.4 | 5.0 | 34.0 | 4.8 | 5.1 | 4.6 |
| TS5 | Spathian (upper Olenekian) | 248 | 3 | 36.835 | 32.487 | 25 | 14/15 | 15.3 | 14.5 | 4.4 | 8.3 | 7.4 | 68.2 | 4.8 | 84.8 | 4.3 | 4.5 | 4.3 | 150/32 | 14/15 | 3.5 | 35.7 | 5.8 | 8.2 | 19.8 | 55.3 | 5.4 | 53.6 | 5.5 | 5.9 | 5.2 |
| TS/TV all specimens | Tournaisian–Olenekian | 295.2 | 50.2 | 36.900 | 32.450 | 148 | 75/79 | 17.4 | 18.2 | 2.3 | 4.3 | 9.3 | 34.0 | 2.8 | 50.9 | 2.3 | 2.4 | 2.3 | 142/29 | 73/79 | 7.1 | 41.1 | 2.9 | 3.5 | 23.6 | 38.8 | 2.7 | 40.9 | 2.6 | 2.6 | 2.5 |
| TS/TV site average | Tournaisian–Olenekian | 295.2 | 50.2 | 36.900 | 32.450 | 148 | 4/4 | 18.0 | 17.6 | 7.7 | 14.1 | 9.0 | 107.3 | 8.9 | 148.0 | 7.6 | 8.1 | 7.3 | 142/29 | 4/4 | 7.3 | 41.4 | 8.8 | 10.9 | 23.8 | 151.3 | 7.5 | 130.5 | 8.1 | 9.1 | 7.4 |
| Fele | | | | | | | | | | | | | | | | | | | | | | | | | | | | | | | |
| FE1 | Bajocian | 169.7 | 1.95 | 37.992 | 31.447 | 24 | 4/6 | 235.3 | −6.6 | 8.5 | 16.8 | 3.3 | 56.3 | 12.4 | 117.8 | 8.5 | 8.9 | 8.5 | 146/36 | 4/6 | 236.1 | −42.3 | 11.3 | 13.6 | 24.5 | 103.7 | 9.1 | 80.5 | 10.3 | 11.9 | 9.2 |
| FE2 | Bajocian–Callovian | 166.4 | 5.2 | 37.991 | 31.447 | 20 | 6/6 | 238.8 | −7.9 | 7.5 | 14.8 | 4.0 | 31.1 | 12.2 | 80.8 | 7.5 | 7.8 | 7.4 | 147/48 | 6/6 | 239.9 | −55.9 | 16.5 | 12.8 | 36.4 | 31.1 | 12.2 | 26.7 | 13.2 | 15.7 | 11.3 |
| FE3 | Malm | 153.35 | 7.85 | 37.988 | 31.445 | 20 | 2/6 | 224.4 | −20.1 | - | - | 10.4 | - | - | - | - | - | - | 146/52 | 2/6 | 221.5 | −46.4 | - | - | 27.7 | - | - | - | - | - | - |
| FE4 | Malm | 153.35 | 7.85 | 37.986 | 31.444 | 20 | 3/4 | 235.2 | −14.2 | 38.1 | 72.1 | 7.2 | 10.0 | 41.3 | 11.7 | 37.8 | 75.4 | 45.8 | 153/46 | 3/4 | 228.3 | −57.5 | 99.9 | 52.9 | 38.1 | 9.8 | 41.8 | 5.8 | 56.6 | 91.5 | 35.8 |
| FE5 | Malm | 153.35 | 7.85 | 37.985 | 31.443 | 20 | 3/6 | 225.8 | −17.5 | 21.7 | 39.9 | 9.0 | 17.2 | 30.7 | 34.2 | 21.4 | 29.1 | 20.6 | 152/40 | 3/6 | 213.5 | −55.7 | 29.3 | 28.6 | 36.2 | 17.9 | 30.1 | 18.7 | 29.3 | 42.4 | 21.9 |
| FE6 | Berriasian–Albian | 122.55 | 22.95 | 37.980 | 37.442 | 21 | 2/6 | 246.4 | −26.2 | - | - | 13.8 | - | - | - | - | - | - | 162/42 | 2/6 | 239.2 | −67.4 | - | - | 50.2 | - | - | - | - | - | - |
| FE7 | Cenomanian | 96.55 | 3.05 | 37.980 | 31.441 | 37 | 4/8 | 253.1 | −9.4 | 12.6 | 24.7 | 4.7 | 27.3 | 17.9 | 54.3 | 12.6 | 14.0 | 12.5 | 156/45 | 4/8 | 256.7 | −53.5 | 23.9 | 20.3 | 34.0 | 25.0 | 18.7 | 22.8 | 19.6 | 25.8 | 15.9 |
| FE8 | Turonian–Maastrichtian | 79.5 | 14 | 37.979 | 31.439 | 20 | 0/6 | | | | | | | | | | | | | 0/6 | | | | | | | | | | | |
| FE9 | Turonian–Maastrichtian | 79.5 | 14 | 37.978 | 31.437 | 18 | 0/6 | | | | | | | | | | | | | 0/6 | | | | | | | | | | | |
| FE all specimens | Dogger–late Cretaceous | 132.6 | 39 | 37.992 | 31.447 | 200 | 23/54 | 239.1 | −11.2 | 5.4 | 10.4 | 5.7 | 21.0 | 6.8 | 32.7 | 5.4 | 5.5 | 5.3 | 158/44 | 24/56 | 235.7 | −54.2 | 9.5 | 7.9 | 34.7 | 21.6 | 6.5 | 15.5 | 7.8 | 8.7 | 7.1 |
| FE site average | Dogger–late Cretaceous | 132.6 | 39 | 37.992 | 31.447 | 200 | 5/7 | 237.7 | −11.2 | 9.7 | 18.7 | 5.7 | 57.5 | 10.2 | 64.4 | 9.6 | 10.4 | 9.4 | 158/44 | 5/7 | 235.3 | −53.8 | 16.4 | 13.8 | 34.3 | 53.4 | 10.6 | 33.3 | 13.4 | 16.2 | 11.6 |

Lat, latitude of the sites; Long, longitude of the site; *N*c, number of collected cores; *N*, number of cores after interpretation and application of a variable cut-off (Vandamme 1994); *N*a, number of analysed samples; *D*, declination; *I*, inclination; Δ*D*x, declination error; $\Delta I_x$, inclination error; λ, palaeolatitude; *k*, estimate of the precision parameter determined from the ChRM directions; $\alpha_{95}$, cone of confidence determined from the ChRM directions; *K*, precision parameter determined from the mean virtual geomagnetic pole (VGP) direction; $A_{95}$, cone of confidence determined from the mean VGP direction. $\Delta\lambda^+$ and $\Delta\lambda^-$ are the errors in palaeolatitude calculated respectively from $I + \Delta I_x$ and $I - \Delta I_x$, with $\Delta I_x$ derived from the $A_{95}$. All values are given before and after correction for bedding tilt. Strike/dip = averaged bedding planes for the samples included in the calculation of the ChRM directions. All specimens/site average: averages and statistics for averaging all individual specimens after applying a variable cut-off (Vandamme 1994) per individual site/for averaging the site means. Sites with less than three specimens were discarded. The large discrepancy between both approaches in the Seydişehir section comes from the relatively large influence of the samples of site TT3.

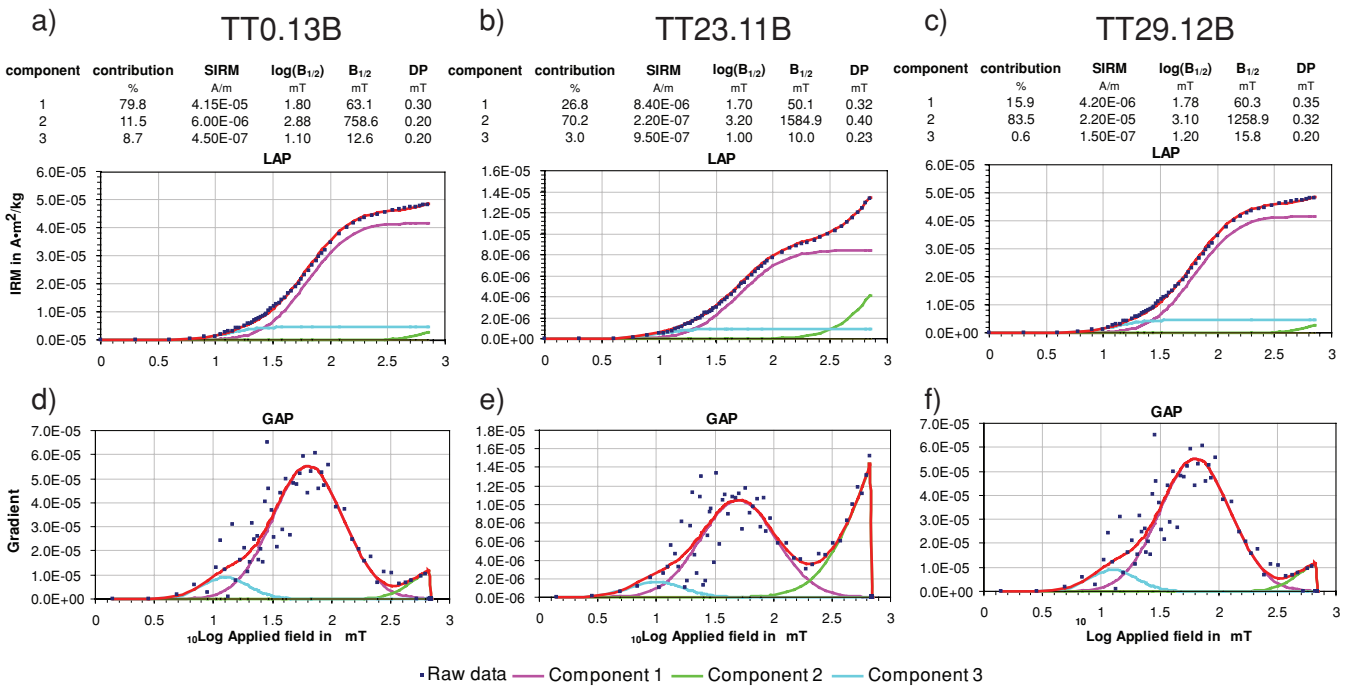


**Figure 7.** (a–c) Examples of IRM component analysis (Kruiver *et al*. 2001) for three typical samples from the Seydişehir section. A legend for the linear acquisition plots (LAP) and gradient acquisition plots (GAP) is given in the figure. The three distinguished components and their contributions, saturation IRM (SIRM), $\log(B_{1/2})$, $B_{1/2}$ and DP are indicated in the tables.

associated with particular grain size distributions that must then be explained in terms of the underlying geological processes.

### *4.2.2 End-member modelling of the IRM acquisition curves*

Inspection of the end-member solutions reveals that the two end-member model has a higher convexity of (−5.0031, after 1000 iterations) and a lower $r^2$ value (0.87) than the three end-member model (Figs 8a and b). The three end-member model (Fig. 8c) has an $r^2$ of 0.90 (final convexity of –2.501, after 1000 iterations), well above the lower limit of 0.80. Models with a number of end-members >3 have only slightly higher $r^2$ values and lower final convexity values (Fig. 8a). In the four and five end-member models, virtual duplication of end-members occurs which makes those models very unattractive form a mathematical point of view. Moreover, those models are difficult to interpret and were discarded. A two end-member model yields a discrimination in a magnetite (with a remagnetized nature, see later on) and hematite end-member (Fig. 8b).

The three end-member model is preferred because it appears to show lithological grouping and it represents the break-in-slope of the $r^2$ versus number of end-members curve (Fig. 8a). The shape of the three end-members (EM 1, 2, 3) is shown in Fig. 8(c) and their partitioning over the samples in Fig. 8(d). They are interpreted along the lines of magnetic minerals. First, we interpret EM3 (yellow) as caused by hematite. Samples that contain a large amount of the HC component in the log-Gaussian approach (Kruiver *et al*. 2001), also contain a substantial portion of EM3.

EM1 (blue in Fig. 8c) is logically interpreted as representing magnetite. The SIRM of this end-member is reached at 500 mT, which is very high for 'classic' magnetite that typically reaches SIRM at 200–300 mT. It is perfectly compatible, however, with the remagnetized magnetite as described by Gong *et al*. (2009a) supporting the remagnetized nature of the present rocks. Gong *et al*. (2009a) showed that non-remagnetized magnetite does not reach saturation fields of 700mT. They proposed magnetically hard behaviour (the absence of magnetic saturation at 700 mT) similar to observations made by Dekkers & Pietersen (1992) for industrial fly ashes that did not reach saturation in fields of 2 T. Transmission electron microscope observations documented closely spaced aggregates of magnetite particles of nominal size of a few nanometres.

The majority of the samples can be seen as mixtures of EM1 and EM3 with only minor contributions of EM2 (purple). The interpretation of EM2 is more complex than that of the other two end-members. It can be a mixture of (relatively soft) magnetite with a tail of hematite. This would be supported by the slightly sandy nature of the limestones with an appreciable EM2 contribution. Alternatively, it could be associated with superparamagnetic magnetite that does not saturate in 700 mT (Gong *et al*. 2009a). The EM2/EM3 ratio is substantially higher in dolomitic limestones and supports this interpretation. In general, dolomitic limestones are associated with high EM1 and low EM3 contributions. The only other site with the same characteristics is site TT39 that consists of shaly limestones.

There is no relation between the EM-distribution and the normal or reversed polarity of the samples. The quality of the demagnetization diagrams does not relate to the end-members either, although dolomitized limestones have higher intensities, and therefore higher quality demagnetization diagrams.

For the interpretation in terms of remagnetization versus non-remagnetization EM3 is not relevant. EM1 reaches saturation at ∼500 mT while EM2 is not yet saturated at the highest field of 700 mT. Importantly, a magnetite end-member that reaches SIRM in 200–300 mT fields is not detected in the present data set. This implies that it is unlikely that we have non-remagnetized magnetite (that would reach SIRM in 200–300 mT (*cf.* Gong *et al*. 2009a; van

**Table 2.** Results of the IRM component analysis (Kruiver *et al*. 2001). In the columns, the three distinguished components and their contributions are shown: saturation IRM (SIRM), log($B_{1/2}$), $B_{1/2}$ and DP.

| | Per cent | $Am^{-12}$ | mT | mT | mT | | Per cent | $Am^{-12}$ | mT | mT | mT |
|---|---|---|---|---|---|---|---|---|---|---|---|
| TT22.6B | | | | | | TT31.20B | | | | | |
| 1 | 77.6 | 1.80E-05 | 1.79 | 61.66 | 0.29 | 1 | 8.7 | 5.60E-06 | 1.79 | 61.66 | 0.36 |
| 2 | 17.2 | 4.00E-06 | 3.00 | 1000.00 | 0.30 | 2 | 91.3 | 5.90E-05 | 3.15 | 1412.54 | 0.36 |
| 3 | 5.2 | 1.20E-06 | 1.12 | 13.18 | 0.14 | 3 | | | | | |
| TT23.11B | | | | | | TT30.19B | | | | | |
| 1 | 26.8 | 8.40E-06 | 1.70 | 50.12 | 0.32 | 1 | 17.9 | 2.30E-06 | 1.83 | 67.61 | 0.35 |
| 2 | 70.2 | 2.20E-05 | 3.20 | 1584.89 | 0.40 | 2 | 81.8 | 1.05E-05 | 2.68 | 478.63 | 0.27 |
| 3 | 3.0 | 9.50E-07 | 1.00 | 10.00 | 0.23 | 3 | 0.2 | 3.00E-08 | 0.99 | 9.77 | 0.05 |
| TT0.13B | | | | | | TT25.11B | | | | | |
| 1 | 79.8 | 4.15E-05 | 1.80 | 63.10 | 0.30 | 1 | 3.3 | 2.40E-06 | 1.73 | 53.70 | 0.31 |
| 2 | 11.5 | 6.00E-06 | 2.88 | 758.58 | 0.20 | 2 | 96.6 | 7.00E-05 | 3.40 | 2511.89 | 0.36 |
| 3 | 8.7 | 4.50E-06 | 1.10 | 12.59 | 0.20 | 3 | 0.1 | 1.00E-07 | 1.20 | 15.85 | 0.07 |
| TT39.2B | | | | | | TT36.15B | | | | | |
| 1 | 95.0 | 1.14E-06 | 1.92 | 83.18 | 0.31 | 1 | 51.3 | 2.00E-06 | 1.75 | 56.23 | 0.30 |
| 2 | | | | | | 2 | 46.2 | 1.80E-06 | 2.89 | 776.25 | 0.30 |
| 3 | 5.0 | 6.00E-08 | 1.15 | 14.13 | 0.28 | 3 | 2.6 | 1.00E-07 | 1.15 | 14.13 | 0.28 |
| TT38.18B | | | | | | TT35.16B | | | | | |
| 1 | 8.0 | 2.80E-06 | 1.95 | 89.13 | 0.67 | 1 | 44.2 | 6.10E-06 | 1.67 | 46.77 | 0.30 |
| 2 | 92.0 | 3.20E-05 | 2.60 | 398.11 | 0.20 | 2 | 52.5 | 7.25E-06 | 2.91 | 812.83 | 0.36 |
| | | | | | | 3 | 3.3 | 4.50E-07 | 1.15 | 14.13 | 0.28 |
| TT32.16B | | | | | | TT34.11B | | | | | |
| 1 | 20.5 | 2.70E-06 | 1.79 | 61.66 | 0.36 | 1 | 38.5 | 2.00E-06 | 1.76 | 57.54 | 0.36 |
| 2 | 79.5 | 1.05E-05 | 2.92 | 831.76 | 0.27 | 2 | 57.7 | 3.00E-06 | 2.99 | 977.24 | 0.35 |
| 3 | | | | | | 3 | 3.8 | 2.00E-07 | 1.00 | 10.00 | 0.30 |
| TT21.20B | | | | | | TT29.12B | | | | | |
| 1 | 71.0 | 7.85E-05 | 1.79 | 61.66 | 0.30 | 1 | 15.9 | 4.20E-06 | 1.78 | 60.26 | 0.35 |
| 2 | 19.0 | 2.10E-05 | 2.95 | 891.25 | 0.30 | 2 | 83.5 | 2.20E-05 | 3.10 | 1258.93 | 0.32 |
| 3 | 10.0 | 1.10E-05 | 1.12 | 13.18 | 0.20 | 3 | 0.6 | 1.50E-07 | 1.20 | 15.85 | 0.20 |
| TT20.1B | | | | | | TT28.17B | | | | | |
| 1 | 77.4 | 2.23E-05 | 1.79 | 61.66 | 0.29 | 1 | 17.0 | 1.55E-06 | 1.85 | 70.79 | 0.29 |
| 2 | 15.6 | 4.50E-06 | 2.48 | 302.00 | 0.22 | 2 | 81.3 | 7.40E-06 | 3.21 | 1621.81 | 0.40 |
| 3 | 6.9 | 2.00E-06 | 1.15 | 14.13 | 0.20 | 3 | 1.6 | 1.50E-07 | 1.35 | 22.39 | 0.20 |
| TT1.9B | | | | | | TT27.17B | | | | | |
| 1 | 75.1 | 2.65E-05 | 1.82 | 66.07 | 0.31 | 1 | 26.6 | 4.05E-06 | 1.73 | 53.70 | 0.31 |
| 2 | 17.0 | 6.00E-06 | 2.88 | 758.58 | 0.30 | 2 | 72.4 | 1.10E-05 | 3.10 | 1258.93 | 0.35 |
| 3 | 7.9 | 2.80E-06 | 1.15 | 14.13 | 0.20 | 3 | 1.0 | 1.50E-07 | 1.35 | 22.39 | 0.20 |
| TT37.15B | | | | | | TT26.12B | | | | | |
| 1 | 12.0 | 1.30E-05 | 1.70 | 50.12 | 0.38 | 1 | 21.1 | 2.70E-06 | 1.74 | 54.95 | 0.30 |
| 2 | 88.0 | 9.50E-05 | 2.95 | 891.25 | 0.36 | 2 | 78.2 | 1.00E-05 | 3.10 | 1258.93 | 0.50 |
| 3 | | | | | | 3 | 0.7 | 9.00E-08 | 0.90 | 7.94 | 0.08 |
| TT33.12B | | | | | | | | | | | |
| 1 | 2.6 | 4.20E-06 | 1.75 | 56.23 | 0.36 | | | | | | |
| 2 | 97.4 | 1.55E-04 | 3.28 | 1905.46 | 0.48 | | | | | | |
| 3 | | | | | | | | | | | |

Hinsbergen *et al*. 2010b). Intriguingly, also in the two end-member model the magnetite EM has a remagnetized nature (it reaches its SIRM at ∼500 mT). Therefore, we conclude that the end-member model interpretation strongly supports the palaeomagnetic interpretation of remagnetized rocks in this transect.

## 5 DISCUSSION

The main result of this study is that the rocks from all three localities that were sampled in the central Taurides, covering a stratigraphy from Carboniferous to at least upper Cretaceous, underwent remagnetization. We will now discuss the implications of this finding in two topics: first the regional extent, the timing and possible causes of remagnetization. Secondly, we will discuss the implications for the previously inferred vertical axis rotations and palaeolatitudinal position of the Taurides in southern Turkey.

### 5.1 Timing and cause of remagnetization

We base our conclusions for remagnetization of the Taurides on palaeomagnetic arguments (reversed polarities in the CNS and similar inclinations from Carboniferous to Cretaceous rocks) and rock magnetic arguments (IRM end-member modelling). Morris & Robertson (1993) argued for remagnetization of the Antalya Nappes, based on palaeomagnetic arguments (negative fold tests, the lack of reversed polarity samples and area-wide consistency of *in situ* mean directions). They argued that this remagnetization event affected also the Beydağları region and that it occurred during Miocene thrusting of the Lycian Nappes over the Beydağları platform. In terms of timing, their interpretation for widespread Miocene remagnetization was recently tested and debated by van Hinsbergen *et al*. (2010a,b) for the Beydağları platform. However, the evidence for remagnetization affecting the Antalya Nappes presented by Morris & Robertson (1993) remains firm. On the other

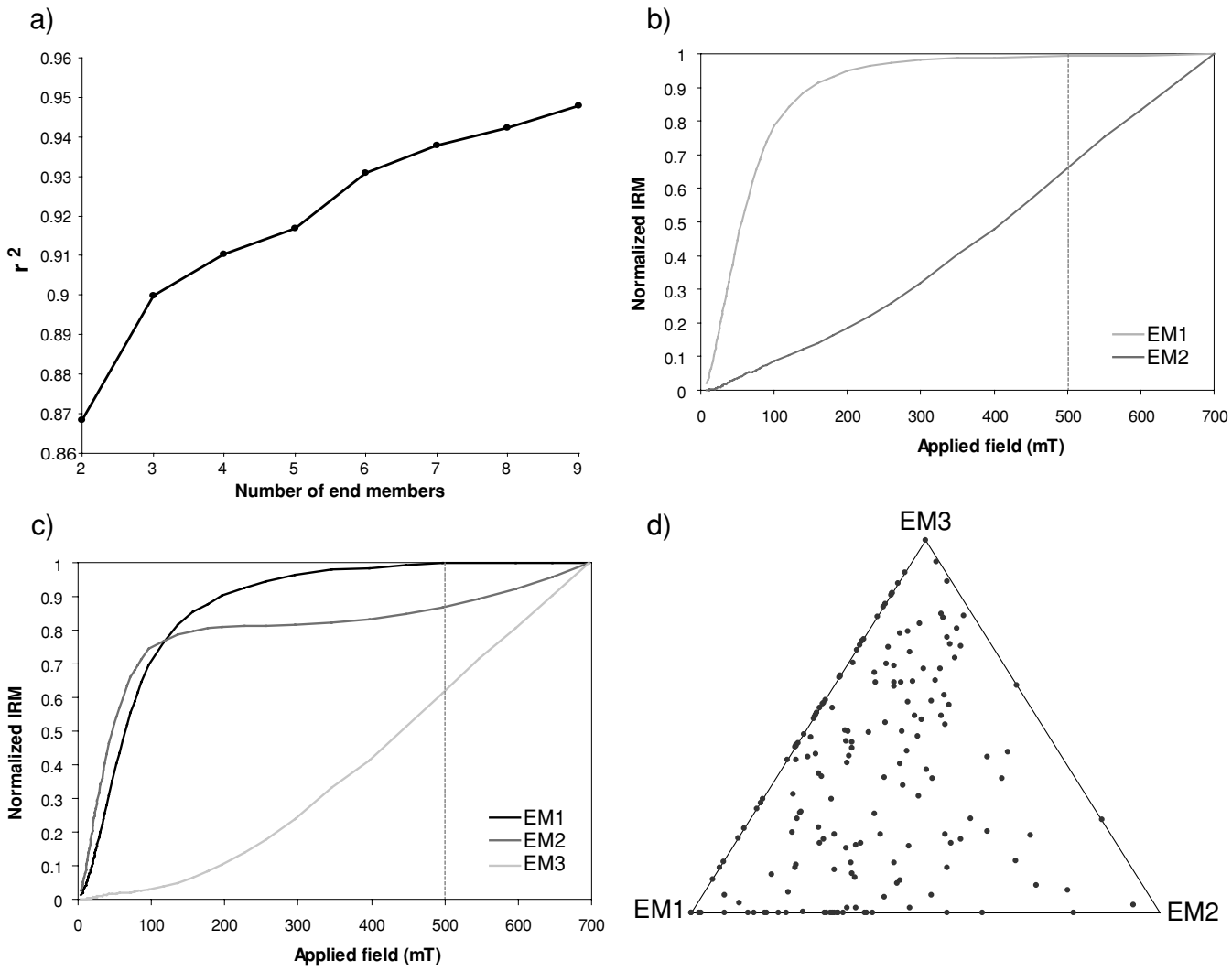


**Figure 8.** (a) Diagram showing the $r^2$ versus number, (b and c) end-member models for the normalized IRM acquisition curves for the two (b) and three (c) end-member models and (d) ternary plot showing percentages of the three end-members in the end-member model per sample.

hand, Gallet *et al*. (1992, 1993, 1994, 1996, 2000, 2007) reported Triassic magnetostratigraphies from the Antalya Nappes, suggesting that not the entire nappe stack was remagnetized. This does not support the widespread, regional nature of this remagnetization event.

The common setting of our sites in the central Taurides fold-and-thrust belt and their close vicinity render it unlikely that remagnetization is widely spaced in time. Therefore, we will assess the possibility of a common remagnetization process and similar timing. The reversed polarities in rocks that were deposited during the CNS demonstrate an age of remagnetization younger than approximately 85 Ma (i.e. the end of the CNS, Ogg *et al*. 2004). Results so far reported from Miocene and younger rocks overlying the Taurides yielded normal and reversed polarities with positive reversal tests (Kissel & Poisson 1986; Kissel *et al*. 1993; van Hinsbergen *et al*. 2010a,b), which demonstrates that there is no reason to assume remagnetization of Miocene deposits. This brackets the timing of remagnetization between 85 and approximately 20 Ma, corresponding to the Burdigalian onset of marine sedimentation on the eastern part of the fold-and-thrust belt (Bassant *et al*. 2005).

As discussed previously, the oldest and structurally the highest nappes in the Taurides include the ophiolites (Bozkır, Antalya and Lycian Nappes) that occur widespread across southern Turkey. The metamorphic soles of the ophiolites are 95–90 Ma, which is older than the maximum age for remagnetization. After the emplacement of the ophiolites, folding and thrusting of the ATB eventually lead to the development of the fold-and-thrust belt in the early Eocene contemporaneous with the deposition of the youngest foreland basin turbidites. This implies that the remagnetization is possibly related to folding and thrusting during the Palaeocene to early Eocene (Özgül 1983) rather than to the ophiolite emplacement at ∼95–90 Ma. Folding and thrusting could also be a candidate for remagnetization in the rocks sampled by Morris & Robertson (1993) in the Antalya Nappes, which underwent nappe stacking in the same time interval (Juteau *et al*. 1977; Robertson & Woodcock 1981; Çelik *et al*. 2006).

Based on the similar inclinations from all sites after tilt correction, remagnetization probably occurred before tilting or during the early stages of tilting, so in the early stages of folding and thrusting. This is further confirmed by the application of a fold test (Tauxe & Watson 1994) and the SCI method (Waldhör & Appel 2006; Gong

*et al*. 2009b) to the data of the Seydişehir section, both suggesting acquisition of the ChRM directions upon ∼65–68 per cent untilting, so in the early stages of folding and thrusting (Data S2) at a latitude of ∼26°N.

If remagnetization occurred after tilting, the *in situ* inclinations should coincide with inclinations one can expect for Eurasia since about 85 Ma (i.e. the maximum age for remagnetization, see above), or they should indicate slightly lower inclinations, because the ATB had not sutured with Eurasia at that times. However, the palaeolatitudes calculated from inclinations of our sections for the *in situ* coordinates are much lower than the Eurasian apparent polar wander path (Torsvik *et al*. 2008) and even lower than the African APWP at the inferred maximum age of remagnetization and are therefore precluded, confirming the results from the fold test and SCI method.

If we apply a full tilt correction, the average calculated palaeolatitudes from Taşkent, Seydişehir and Fele (shaded squares, Fig. 9) suggest a palaeolatitude that is close to the latitude of Europe during collision, that is, during the late Cretaceous to early Palaeogene. This strengthens the suggestion that the remagnetization occurred in the early stages of folding.

Several mechanisms and settings have previously been invoked to explain remagnetization, broadly speaking in two main categories: viscous resetting of existing magnetic minerals at burial temperatures for the duration of the burial (thermoviscous remagnetization; Kent 1985). If prevailing burial temperatures are too low to make this model plausible, neoformation of magnetic minerals by chemical remanent magnetization (McCabe & Elmore 1989) may be an alternative. Fluids are presumed to have delivered the constituents for the newly formed magnetic minerals. Morris & Robertson (1993) suggested that 'orogenic fluids' remagnetized the Antalya Nappes. More recent remagnetization studies, however, are more conservative and do not invoke (large amounts of) external fluid (Katz *et al*. 1998; Machel & Cavell 1999; Katz *et al*. 2000; Blumstein *et al*. 2004). These latter studies document that diagenetic reactions deliver the iron required to form magnetite, amongst others by reactions involving clay minerals obviating the need for external fluids. When dolomitization of the carbonates is occurring, evolved fluid is reported to have migrated in relation to remagnetization (O'Brien *et al*. 2007). The role of pressure solution in remagnetization, although equivocal (Evans *et al*. 2003; Elmore *et al*. 2006), could be a likely mechanism in the case of the Taurides fold-and-thrust belt, because stylolites are frequently observed (Gong *et al*. 2008a).

In other words, it is most likely that the remagnetization was somehow the result of fluids or pressure build-up reactions invoked by folding and thrusting. Given the continuous sedimentation of the Seydişehir section into the Palaeocene to lower Eocene foreland basin deposits, the timing of remagnetization is likely Eocene, and may have influenced all Eocene and older folded and thrusted rocks in the central Taurides axis, including those that were used by Kissel *et al*. (1993) to analyse the Taurides rotation history.

### 5.2 Implications for regional rotations

Results from previous palaeomagnetic studies on Ordovician to Pleistocene rocks in the western and central Taurides are listed in Table 3. These studies were conducted for a variety of purposes, including magnetostratigraphy, rotation and palaeolatitude studies. In Figs 2(a)–(c), we indicate the rotation results from all published sites in three time slices (Palaeozoic to Palaeogene, Miocene and Pliocene to Pleistocene). Because we argue that the rocks of this study were all remagnetized in the late Cretaceous to Eocene, we displayed them in Fig. 2(a) (Palaeogene). Our data are combined in

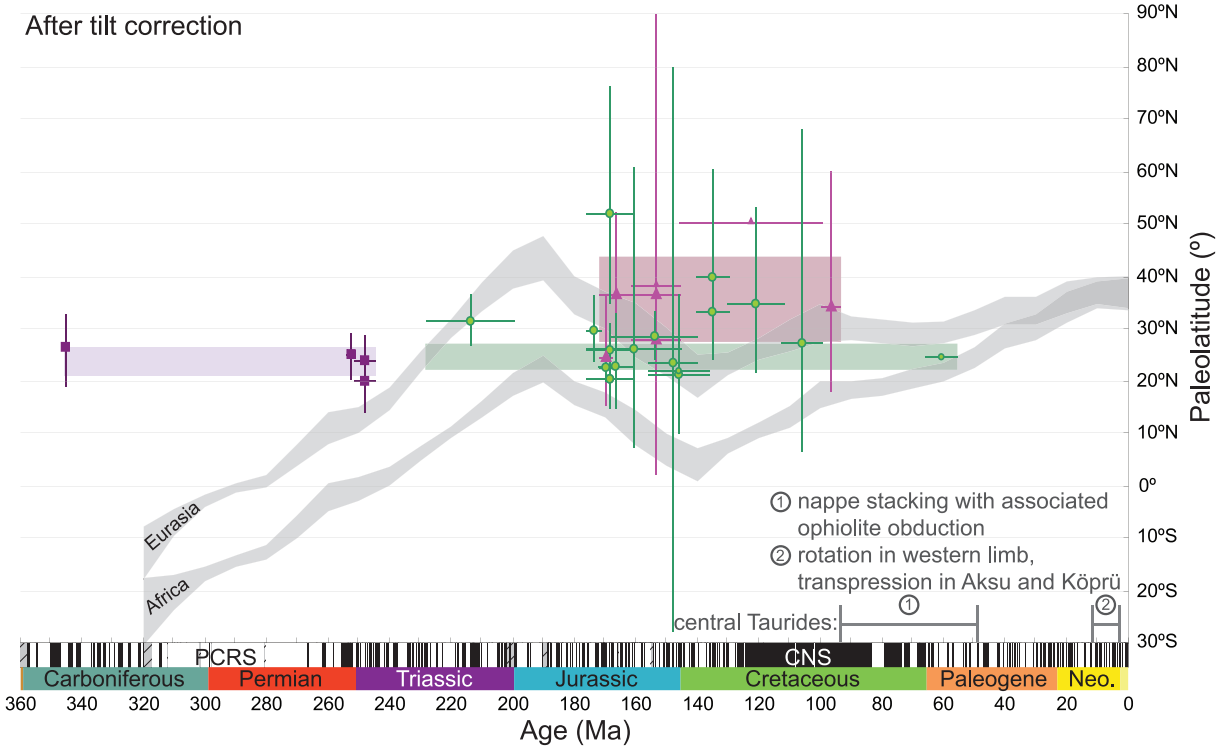


**Figure 9.** Age versus latitute plots of all Tauride data from this study after tilt correction. Purple squares, data from the Taskent sites; green circles, data from the Seydisehir section; pink triangles, data from the Fele section. Large shaded squares indicate the average palaeolatitude with its error for each area or site. Grey shaded curves: APW path of Torsvik *et al*. (2008) with its $A_{95}$ error from 320–0 Ma. Below the curves the magnetic polarity timescale (Ogg *et al*. 2008) is indicated. PCRS, Permo-Carboniferous Reversed Superchrom; CNS, Cretaceous Normal Superchron; Neo., Neogene.

**Table 3.** Table showing data from previously published studies.

| Site | Lat | Long | Age | Age error | $N$ | $D$ | $I$ | $k$ | $\alpha_{95}$ | $\lambda$ | $K_{(VGP)}$ | $A_{95(vgp)}$ | $\Delta I_x$ | $\Delta D_x$ | $\Delta\lambda^+$ | $\Delta\lambda^-$ | Authors |
|---|---|---|---|---|---|---|---|---|---|---|---|---|---|---|---|---|---|
| Pliocene–Pleistocene | | | | | | | | | | | | | | | | | |
| IS29 | 37.7 | 30.7 | 1.3 | 0.5 | 8 | 5.3 | 59.0 | 170.0 | 3.7 | 39.8 | 98.0 | 5.6 | 5.0 | 7.3 | 6.7 | 5.8 | Kissel & Poisson (1986) |
| IS31 | 37.7 | 30.7 | 1.3 | 0.5 | 9 | 358.0 | 58.0 | 288.0 | 2.7 | 38.7 | 172.0 | 3.9 | 3.6 | 5.0 | 4.5 | 4.1 | Kissel & Poisson (1986) |
| BU 1 | 37.7 | 30.3 | 1.3 | 0.5 | 9 | 177.8 | −57.7 | | | 38.3 | | 10.8 | 10.0 | 13.8 | 12.3 | 9.6 | van Hinsbergen *et al.* (2010a) |
| AN37 | 36.9 | 30.9 | 2.7 | 0.9 | 9 | 186.0 | −48.0 | 270.0 | 2.8 | 29.0 | 221.7 | 3.5 | 4.1 | 4.0 | 3.1 | 2.8 | Kissel & Poisson (1986) |
| AN40 | 36.8 | 31.3 | 3.6 | 1.8 | 10 | 358.0 | 52.0 | 107.0 | 4.0 | 32.6 | 77.9 | 5.5 | 5.9 | 6.5 | 5.5 | 4.8 | Kissel & Poisson (1986) |
| IP[a] | 37.8 | 30.8 | 4.4 | 0.4 | 20 | 5.8 | 52.6 | 40.1 | 6.1 | 33.2 | 28.6 | 6.2 | 6.5 | 7.4 | 6.7 | 5.8 | Tatar *et al.* (2002) |
| IS04 | 37.7 | 30.5 | 4.5 | 0.9 | 9 | 12.5 | 46.6 | 221.0 | 3.0 | 27.9 | 188.8 | 3.8 | 4.5 | 4.2 | 3.2 | 3.0 | Kissel & Poisson (1986) |
| AN39 | 37.1 | 30.8 | 4.5 | 0.9 | 8 | 182.0 | −52.0 | 19.0 | 11.0 | 32.6 | 13.8 | 15.4 | 16.5 | 18.4 | 17.7 | 12.3 | Kissel & Poisson (1986) |
| DB[a] | 37.6 | 32.0 | 5.2 | 1.7 | 4 | 359.0 | 50.8 | 33.4 | 13.4 | 31.5 | 25.2 | 18.7 | 20.5 | 22.0 | 24.4 | 15.2 | Tatar *et al.* (2002) |
| Late Miocene | | | | | | | | | | | | | | | | | |
| KE 1 | 37.2 | 29.3 | 6.7 | 4.9 | 8 | 186.2 | −23.7 | | | 12.4 | | 22.1 | 38.8 | 22.7 | 31.5 | 20.1 | van Hinsbergen *et al.* (2010a) |
| KE 2 | 37.2 | 29.4 | 6.7 | 4.9 | 9 | 354.6 | 59.6 | | | 40.4 | | 11.3 | 10.0 | 14.9 | 12.9 | 10.0 | van Hinsbergen *et al.* (2010a) |
| KE 3 | 37.2 | 29.4 | 6.7 | 4.9 | 12 | 336.2 | 57.0 | | | 37.6 | | 9.3 | 8.8 | 11.8 | 10.4 | 8.4 | van Hinsbergen *et al.* (2010a) |
| KE 4 | 37.2 | 29.3 | 6.7 | 4.9 | 20 | 343.3 | 54.1 | | | 34.6 | | 8.1 | 8.2 | 9.9 | 9.0 | 7.4 | van Hinsbergen *et al.* (2010a) |
| IO[a] | 39.5 | 30.3 | 9.3 | 3.0 | 13 | 191.5 | −55.7 | 16.4 | 10.6 | 36.2 | 10.6 | 13.4 | 13.0 | 16.7 | 15.9 | 11.5 | Gürsoy *et al.* (2003) |
| DH[a] | 37.7 | 32.1 | 9.9 | 1.0 | 14 | 182.5 | −46.7 | 25.6 | 9.7 | 27.9 | 21.8 | 8.7 | 10.5 | 9.9 | 9.9 | 7.8 | Tatar *et al.* (2002) |
| IS32 | 37.6 | 30.7 | 10.5 | 3.2 | 8 | 352.0 | 43.0 | 163.0 | 4.0 | 25.0 | 153.4 | 4.5 | 5.8 | 5.0 | 3.6 | 3.3 | Kissel & Poisson (1986) |
| AN33 | 36.7 | 31.8 | 10.5 | 3.2 | 9 | 359.0 | 54.4 | 24.0 | 9.5 | 34.9 | 16.2 | 13.2 | 13.3 | 16.2 | 15.6 | 11.3 | Kissel & Poisson (1986) |
| SW[a] | 38.6 | 30.4 | 11.0 | 3.0 | 10 | 192.2 | −48.8 | 20.5 | 10.9 | 29.7 | 16.4 | 12.3 | 14.1 | 14.2 | 14.6 | 10.7 | Gürsoy *et al.* (2003) |
| SI[a] | 37.7 | 32.1 | 11.6 | 0.1 | 5 | 149.5 | −51.8 | 67.6 | 11.3 | 32.4 | 49.5 | 11.0 | 11.8 | 13.0 | 12.8 | 9.7 | Tatar *et al.* (2002) |
| IC[a] | 38.8 | 31.0 | 11.6 | 0.2 | 7 | 196.5 | −46.5 | 27.7 | 11.7 | 27.8 | 23.7 | 12.6 | 15.3 | 14.3 | 15.2 | 10.9 | Gürsoy *et al.* (2003) |
| Middle Miocene | | | | | | | | | | | | | | | | | |
| ED[a] | 38.7 | 31.3 | 13.0 | 5.0 | 11 | 205.1 | −42.1 | 10.7 | 14.6 | 24.3 | 10.3 | 14.9 | 19.8 | 16.4 | 18.8 | 12.7 | Gürsoy *et al.* (2003) |
| TK192 | 36.7 | 33.0 | 14.2 | 8.9 | 11 | 5.0 | 50.0 | 97.0 | 4.6 | 30.8 | 75.1 | 5.3 | 5.9 | 6.2 | 5.0 | 4.5 | Kissel *et al.* (1993) |
| TK193 | 36.7 | 33.0 | 14.2 | 8.9 | 8 | 350.0 | 56.0 | 268.0 | 3.4 | 36.5 | 171.3 | 4.2 | 4.1 | 5.3 | 4.6 | 4.2 | Kissel *et al.* (1993) |
| TK194 | 36.7 | 33.0 | 14.2 | 8.9 | 9 | 1.0 | 54.0 | 369.0 | 2.8 | 34.5 | 252.0 | 3.2 | 3.3 | 3.9 | 3.3 | 3.1 | Kissel *et al.* (1993) |
| AN34 | 37.8 | 31.8 | 14.8 | 1.2 | 4 | 11.3 | 38.4 | 23.0 | 14.0 | 21.6 | 24.2 | 19.1 | 27.1 | 20.6 | 16.5 | 11.7 | Kissel & Poisson (1986) |
| AN35 | 36.7 | 31.8 | 14.8 | 1.2 | 9 | 347.0 | 59.0 | 49.0 | 7.0 | 39.8 | 28.3 | 9.9 | 8.8 | 12.9 | 12.5 | 9.7 | Kissel & Poisson (1986) |
| Early Miocene | | | | | | | | | | | | | | | | | |
| EL70 | 37.0 | 29.7 | 17.4 | 5.6 | 10 | 161.0 | −30.0 | 39.0 | 7.0 | 16.1 | 48.5 | 7.0 | 11.4 | 7.3 | 4.5 | 4.1 | Kissel & Poisson (1987) |
| EL73 | 37.1 | 30.2 | 17.4 | 5.6 | 9 | 324.0 | 39.0 | 57.0 | 6.0 | 22.0 | 59.1 | 6.8 | 9.5 | 7.3 | 5.1 | 4.5 | Kissel & Poisson (1987) |
| EL78 | 36.4 | 29.7 | 17.4 | 5.6 | 7 | 359.0 | 68.0 | 39.0 | 18.0 | 51.1 | 16.3 | 15.4 | 11.0 | 25.0 | 26.0 | 17.9 | Kissel & Poisson (1987) |
| Korkuteli (KL) | 37.1 | 30.1 | 17.4 | 5.6 | 340 | 339.5 | 45.5 | | | 27.0 | | 2.2 | 2.7 | 2.5 | 4.9 | 4.3 | van Hinsbergen *et al.* (2010a,b,c) |
| Dogantas I (DT1) | 36.5 | 29.9 | 17.4 | 5.6 | 35 | 347.4 | 41.7 | | | 24.0 | | 16.6 | 22.2 | 18.2 | 15.0 | 10.8 | van Hinsbergen *et al.* (2010a,b,c) |
| Dogantas II (DT2) | 36.5 | 29.9 | 17.4 | 5.6 | 38 | 320.2 | 48.1 | | | 29.1 | | 10.3 | 12.0 | 11.8 | 10.0 | 7.9 | van Hinsbergen *et al.* (2010a,b,c) |
| Dogantas III (DT3) | 36.5 | 29.9 | 17.4 | 5.6 | 61 | 330.5 | 42.9 | | | 24.9 | | 14.8 | 19.3 | 16.4 | 13.4 | 10.0 | van Hinsbergen *et al.* (2010a,b,c) |
| IH[a] | 39.1 | 30.6 | 18.7 | 1.4 | 9 | 197.0 | −44.0 | 45.7 | 7.7 | 25.8 | 41.9 | 8.0 | 10.3 | 8.9 | 9.0 | 7.3 | Gürsoy *et al.* (2003) |
| AC[a] | 37.4 | 29.3 | 19.5 | 3.5 | 7 | 351.3 | 48.4 | | | 29.4 | 51.2 | 3.0 | 3.4 | 3.4 | 3.0 | 2.8 | van Hinsbergen *et al.* (2010a) |
| Palaeogene | | | | | | | | | | | | | | | | | |
| EL67 | 36.8 | 30.0 | 28.5 | 5.5 | 7 | 333.0 | 40.0 | 55.0 | 7.0 | 22.8 | 55.7 | 8.2 | 11.3 | 8.9 | 6.4 | 5.5 | Kissel & Poisson (1987) |
| YA | 37.2 | 30.5 | 44.3 | 21.2 | 27 | 312.0 | 39.0 | 15.0 | 7.4 | 22.0 | 15.6 | 7.3 | 10.2 | 7.9 | 5.6 | 4.9 | Morris & Robertson (1993) |
| CD | 37.6 | 30.7 | 44.3 | 21.2 | 5 | 352.0 | 42.0 | 21.0 | 16.9 | 24.2 | 20.3 | 17.4 | 23.1 | 19.2 | 16.0 | 11.3 | Morris & Robertson (1993) |

**Table 3.** (*Continued.*)

| Site | Lat | Long | Age | Age error | $N$ | $D$ | $I$ | $k$ | $\alpha_{95}$ | $\lambda$ | $K_{(VGP)}$ | $A_{95(vgp)}$ | $\Delta I_x$ | $\Delta D_x$ | $\Delta\lambda^+$ | $\Delta\lambda^-$ | Authors |
|---|---|---|---|---|---|---|---|---|---|---|---|---|---|---|---|---|---|
| EL83 | 37.5 | 30.5 | 44.9 | 11.0 | 6 | 115.0 | −16.0 | 19.0 | 13.0 | 8.2 | 28.3 | 12.8 | 24.2 | 12.9 | 7.2 | 6.6 | Kissel & Poisson (1987) |
| EL 84 | 37.2 | 30.3 | 44.9 | 11.0 | 8 | 154.0 | −29.0 | 61.0 | 6.0 | 15.5 | 77.1 | 6.3 | 10.5 | 6.6 | 4.0 | 3.7 | Kissel & Poisson (1987) |
| EL71 | 37.1 | 30.2 | 44.9 | 11.0 | 8 | 340.0 | 32.0 | 54.0 | 6.0 | 17.4 | 64.7 | 6.9 | 10.9 | 7.3 | 4.6 | 4.2 | Kissel & Poisson (1987) |
| TK176 | 37.1 | 31.8 | 44.9 | 11.0 | 9 | 223.0 | −15.0 | 38.0 | 7.5 | 7.6 | 57.1 | 6.9 | 13.0 | 6.9 | 3.7 | 3.5 | Kissel *et al.* (1993) |
| TK177 | 37.1 | 31.6 | 44.9 | 11.0 | 7 | 231.0 | −28.0 | 27.0 | 11.9 | 14.9 | 34.7 | 10.4 | 17.4 | 10.8 | 6.7 | 5.9 | Kissel *et al.* (1993) |
| TK178 | 37.1 | 31.8 | 44.9 | 11.0 | 8 | 212.0 | −21.0 | 18.0 | 13.6 | 10.9 | 25.5 | 11.2 | 20.2 | 11.4 | 6.6 | 5.9 | Kissel *et al.* (1993) |
| TK179 | 37.1 | 31.8 | 44.9 | 11.0 | 7 | 233.0 | −17.0 | 47.0 | 7.7 | 8.7 | 69.4 | 7.3 | 13.7 | 7.4 | 4.0 | 3.8 | Kissel *et al.* (1993) |
| TK180 | 37.0 | 31.8 | 44.9 | 11.0 | 10 | 213.0 | −30.0 | 21.0 | 9.6 | 16.1 | 26.1 | 9.6 | 15.7 | 10.0 | 6.4 | 5.6 | Kissel *et al.* (1993) |
| TK196 | 36.6 | 32.9 | 44.9 | 11.0 | 11 | 13.0 | 49.0 | 79.0 | 5.2 | 29.9 | 63.0 | 5.8 | 6.6 | 6.7 | 5.4 | 4.8 | Kissel *et al.* (1993) |
| TK197 | 36.7 | 32.8 | 44.9 | 11.0 | 12 | 38.0 | 50.0 | 114.0 | 4.1 | 30.8 | 88.2 | 4.6 | 5.2 | 5.4 | 4.4 | 3.9 | Kissel *et al.* (1993) |
| LE | 38.0 | 30.8 | 49.7 | 15.8 | 6 | 335.0 | 29.0 | 46.0 | 10.0 | 15.5 | 58.1 | 8.9 | 14.6 | 9.2 | 5.7 | 5.1 | Morris & Robertson (1993) |
| TK185 | 37.4 | 31.5 | 60.7 | 4.9 | 9 | 233.0 | −6.0 | 45.0 | 7.8 | 3.0 | 71.3 | 6.1 | 12.2 | 6.1 | 3.1 | 3.1 | Kissel *et al.* (1993) |
| TK190 | 37.3 | 31.8 | 60.7 | 4.9 | 5 | 41.0 | 48.0 | 14.0 | 23.0 | 29.0 | 11.5 | 23.6 | 27.6 | 27.2 | 27.3 | 16.2 | Kissel *et al.* (1993) |
| DA | 36.4 | 30.2 | 60.7 | 4.9 | 4 | 344.0 | 44.0 | 40.0 | 14.7 | 25.8 | 36.7 | 15.4 | 19.6 | 17.1 | 14.4 | 10.5 | Morris & Robertson (1993) |
| FI | 36.5 | 30.1 | 60.7 | 4.9 | 12 | 354.0 | 40.0 | 30.0 | 7.9 | 22.8 | 30.4 | 8.0 | 11.0 | 8.7 | 6.3 | 5.4 | Morris & Robertson (1993) |
| DK | 36.9 | 30.3 | 60.7 | 4.9 | 8 | 349.0 | 45.0 | 21.0 | 12.3 | 26.6 | 18.8 | 13.1 | 16.4 | 14.7 | 12.2 | 9.3 | Morris & Robertson (1993) |
| Paleozoic–Mesozoic | | | | | | | | | | | | | | | | | |
| KA | 37.7 | 31.1 | 77.4 | 11.9 | 4 | 15.0 | 17.0 | 47.0 | 13.6 | 8.7 | 69.4 | 11.1 | 20.8 | 11.2 | 6.3 | 5.7 | Morris & Robertson (1993) |
| KO | 37.9 | 31.0 | 82.6 | 17.1 | 7 | 328.0 | 44.0 | 47.0 | 8.9 | 25.8 | 43.1 | 9.3 | 11.9 | 10.3 | 8.1 | 6.7 | Morris & Robertson (1993) |
| KK4 | 36.6 | 30.5 | 132.6 | 67.1 | 40 | 30.0 | 40.0 | 27.0 | 4.5 | 22.8 | 27.4 | 4.4 | 6.1 | 4.8 | 3.3 | 3.1 | Morris & Robertson (1993) |
| Akseki 1 (AK1) | 37.0 | 31.5 | 148.2 | 2.7 | 49 | 303.0 | −9.0 | 11.0 | 6.0 | 4.5 | 17.2 | 5.1 | 9.9 | 5.1 | 2.6 | 2.6 | Piper *et al.* (2002) |
| Felepinar 5 (FP5) | 37.6 | 31.3 | 158.5 | 2.8 | 9 | 289.0 | −24.0 | 10.0 | 17.0 | 12.6 | 13.6 | 14.5 | 25.3 | 14.8 | 9.1 | 7.7 | Piper *et al.* (2002) |
| Bagpinar 6 (BP6) | 38.1 | 31.2 | 158.5 | 2.8 | 9 | 186.0 | −12.0 | 22.0 | 11.0 | 6.1 | 33.8 | 9.0 | 17.4 | 9.0 | 4.8 | 4.6 | Piper *et al.* (2002) |
| Bagpinar 7 (BP7) | 38.1 | 31.2 | 158.5 | 2.8 | 4 | 162.0 | −31.0 | 39.0 | 15.0 | 16.7 | 47.6 | 13.5 | 21.6 | 14.1 | 9.4 | 7.7 | Piper *et al.* (2002) |
| Akseki 2 (AK2) | 37.1 | 31.5 | 179.3 | 3.7 | 7 | 276.0 | 23.0 | 16.0 | 15.0 | 12.0 | 22.1 | 13.1 | 23.2 | 13.4 | 8.1 | 7.0 | Piper *et al.* (2002) |
| Akseki 3 (AK3) | 37.1 | 31.5 | 179.3 | 3.7 | 6 | 256.0 | 8.0 | 35.0 | 12.0 | 4.0 | 55.0 | 9.1 | 18.0 | 9.1 | 4.7 | 4.6 | Piper *et al.* (2002) |
| Felepinar 4 (FP4) | 38.0 | 31.3 | 187.6 | 12.0 | 7 | 278.0 | −11.0 | 18.0 | 15.0 | 5.6 | 27.9 | 11.6 | 22.6 | 11.7 | 6.2 | 5.9 | Piper *et al.* (2002) |
| Oyuklu section (OY) | 36.7 | 32.9 | 204.8 | 5.2 | 106 | 327.9 | 37.9 | 21.1 | 3.1 | 21.3 | 22.4 | 3.0 | 4.2 | 3.2 | 2.1 | 2.0 | Gallet *et al.* (1993) |
| Kavur Tepe (KT) | 38.0 | 30.8 | 210.5 | 6.5 | 179 | 220.2 | 32.1 | 40.9 | 1.7 | 17.4 | 49.0 | 1.5 | 2.4 | 1.6 | 1.0 | 1.0 | Gallet *et al.* (1993) |
| Kavaalani Section (KV) | 36.3 | 30.3 | 212.0 | 8.0 | 163 | 209.5 | 18.6 | 17.2 | 2.7 | 9.6 | 25.0 | 2.3 | 4.2 | 2.3 | 1.2 | 1.2 | Gallet *et al.* (2000) |
| HA | 37.0 | 30.4 | 213.3 | 37.7 | 37 | 37.0 | 12.0 | 13.0 | 6.9 | 6.1 | 20.0 | 5.4 | 10.5 | 5.4 | 2.8 | 2.8 | Morris & Robertson (1993) |
| BA | 38.0 | 30.7 | 213.8 | 14.2 | 9 | 320.0 | 25.0 | 19.0 | 12.1 | 13.1 | 25.5 | 10.4 | 18.0 | 10.7 | 6.4 | 5.7 | Morris & Robertson (1993) |
| CI | 36.4 | 30.4 | 213.8 | 14.2 | 18 | 309.0 | −46.0 | 10.0 | 11.8 | 27.4 | 8.7 | 12.4 | 15.2 | 14.0 | 11.8 | 9.0 | Morris & Robertson (1993) |
| Bolucektasi Tepe 2 (BT2) | 36.5 | 30.5 | 215.0 | 5.0 | 172 | 59.3 | 20.1 | 41.8 | 1.7 | 10.4 | 59.8 | 1.4 | 2.6 | 1.4 | 0.8 | 0.8 | Gallet *et al.* (1992) |
| Erenkolu Mezarlik 2 (EM2) | 36.7 | 30.6 | 219.5 | 2.5 | 24 | 223.7 | −25.2 | 37.3 | 4.8 | 13.2 | 50.0 | 4.2 | 7.3 | 4.3 | 2.5 | 2.4 | Gallet *et al.* (1994) |
| AN | 37.9 | 31.0 | 222.3 | 22.7 | 13 | 320.0 | 68.0 | 37.0 | 6.9 | 51.1 | 15.4 | 10.9 | 7.7 | 17.5 | 17.5 | 13.4 | Morris & Robertson (1993) |
| Bolucektasi Tepe 1 (BT1) | 36.5 | 30.5 | 225.0 | 3.0 | 60 | 211.0 | −11.0 | 27.1 | 3.6 | 5.6 | 41.9 | 2.9 | 5.6 | 2.9 | 1.5 | 1.5 | Gallet *et al.* (1992) |
| Erenkolu Mezarlik 1 (EM1) | 36.7 | 30.6 | 225.0 | 3.0 | 24 | 20.7 | 21.1 | 45.0 | 4.5 | 10.9 | 63.6 | 3.7 | 6.7 | 3.8 | 2.1 | 2.0 | Gallet *et al.* (1994) |
| KK3 | 36.6 | 30.5 | 225.3 | 25.7 | 7 | 55.0 | 20.0 | 8.0 | 22.0 | 10.3 | 11.5 | 18.6 | 34.0 | 18.9 | 11.5 | 9.6 | Morris & Robertson (1993) |
| Bademli redbeds (BR) | 37.3 | 31.7 | 259.0 | 59.0 | 19 | 41.0 | 13.5 | 22.0 | 7.8 | 6.8 | 33.5 | 5.9 | 11.3 | 5.9 | 3.1 | 3.0 | Van der Voo & Van der Kleijn (1970) |
| KK2 | 36.6 | 30.5 | 275.0 | 24.0 | 49 | 49.0 | 26.0 | 15.0 | 5.3 | 13.7 | 19.9 | 4.7 | 8.0 | 4.8 | 2.8 | 2.7 | Morris & Robertson (1993) |
| KK1 | 36.6 | 30.5 | 466.0 | 22.3 | 27 | 112.0 | 29.0 | 13.0 | 7.9 | 15.5 | 16.4 | 7.1 | 11.6 | 7.3 | 4.5 | 4.1 | Morris & Robertson (1993) |

[a]N refers to number of combined sites of these studies, the actual amount of demagnetized specimens is lower.

Lat, latitude of the sites; Long, longitude of the site; $N$, number of samples; $D$, declination; $I$, inclination; $k$, estimate of the precision parameter determined from the ChRM directions; $\alpha_{95}$, cone of confidence determined from the ChRM directions; $\lambda$, palaeolatitude; $K_{(vgp)}$, precision parameter determined from the mean virtual geomagnetic pole (VGP) direction; $A_{95(VGP)}$, cone of confidence determined from the mean VGP direction; $\Delta I$x, inclination error; $\Delta D$x, declination error. $\Delta\lambda^+$ and $\Delta\lambda^-$ are the errors in palaeolatitude calculated from the $A_{95}$.

three group means (FE, TT and TS–TV), since the sampled areas are relatively small.

In an analysis of our new and published data, we exclude data sets that do not have a minimum number of samples. In sediments, the minimum number of samples is five; in the case that volcanic rocks were sampled, the required number of flows/sites (with a minimum of demagnetized specimens per lava flow $\geq 5$) that constitute one locality is five, to allow averaging of the secular variation. The accepted sites are indicated in Table 3 and their results are displayed in Figs 2(a)–(c) and 10. From the published data, 10 out of 65 data sets were rejected.

The first time interval covers the Palaeozoic to Mesozoic and Palaeogene (Fig. 2a) and thus includes syn-collisional and younger rotations. The second interval (early to middle Miocene and late Miocene; Fig. 2b) marks a post-collisional deformation phase, which relates to the advance of the Lycian Nappes in the west, and should also include the rotations related to the Isparta Angle formation. The youngest interval (Pliocene to Pleistocene; Fig. 2c) post-dates the time span of the Isparta Angle formation [middle Miocene (Langhian) to latest Miocene; van Hinsbergen *et al*. (2010a)].

Morris & Robertson (1993) argue that their Palaeozoic to Palaeogene data are all remagnetized (except for sites LE and BA). Therefore, these data should be presented in Fig. 2(a) in *in situ* coordinates. Recently, however, van Hinsbergen *et al*. (2010b) argued that remagnetization is likely not the case fore the data sets presented by Morris & Robertson (1993) from Beydağları. Therefore, we display these data (CD, DK, FI, DA, YA) after tilt correction. Possibly, also site KO is not remagnetized, considering that the post-tilt direction is very consistent with both BA and LE. Therefore, we display this site after correction for bedding attitude. Sites AN, KA and CI are certainly remagnetized and were therefore displayed in *in situ* coordinates (blue in Fig. 2a). Sites HA and KK1–4 are possibly remagnetized and therefore we displayed them in both *in situ* and tilt-corrected coordinates.

This is of importance when discussing the Palaeozoic to Mesozoic data (Fig. 2a) that in general show a dispersed pattern, except for the southwestern Antalya Nappes. Here, a general clockwise rotation of $\sim 40^{\circ}$ is visible in the data sets from Morris & Robertson (1993) and Gallet *et al*. (1992, 1994, 2000), when they are all corrected for bedding tilt (with the exception of the Ordovician site KK1 in Fig. 2a). This is rather remarkable, because these clockwise rotations are in agreement with rotations in the central Tauride belt. In particular, all Triassic sites from the southwestern Antalya Nappes, both those of Gallet *et al*. (1992, 1994, 2000, KV, BT1–2, EM1–2) and those of Morris & Robertson (1993) (HA, KK3), are remarkably consistent, and the calculated palaeolatitudes plot within error on the African apparent polar wander path (Fig. 10, Torsvik *et al*. 2008). Site BA, located in the northern Antalya Nappes also yields a palaeolatitude that agrees very well with the African apparent polar wander path.

On the contrary, if we do not correct the sites from the southwestern Antalya Nappes (KK2–4 and CI) of Morris & Robertson (1993) for bedding tilt, they show exactly opposite rotations to the rotations reported by Gallet *et al*. (1992, 1994, 2000), but they agree very well with the rotation in Beydağları and the Lycian Nappes. It is therefore possible that at least the Triassic sites (except CI) are not remagnetized, but a more detailed study on remagnetization

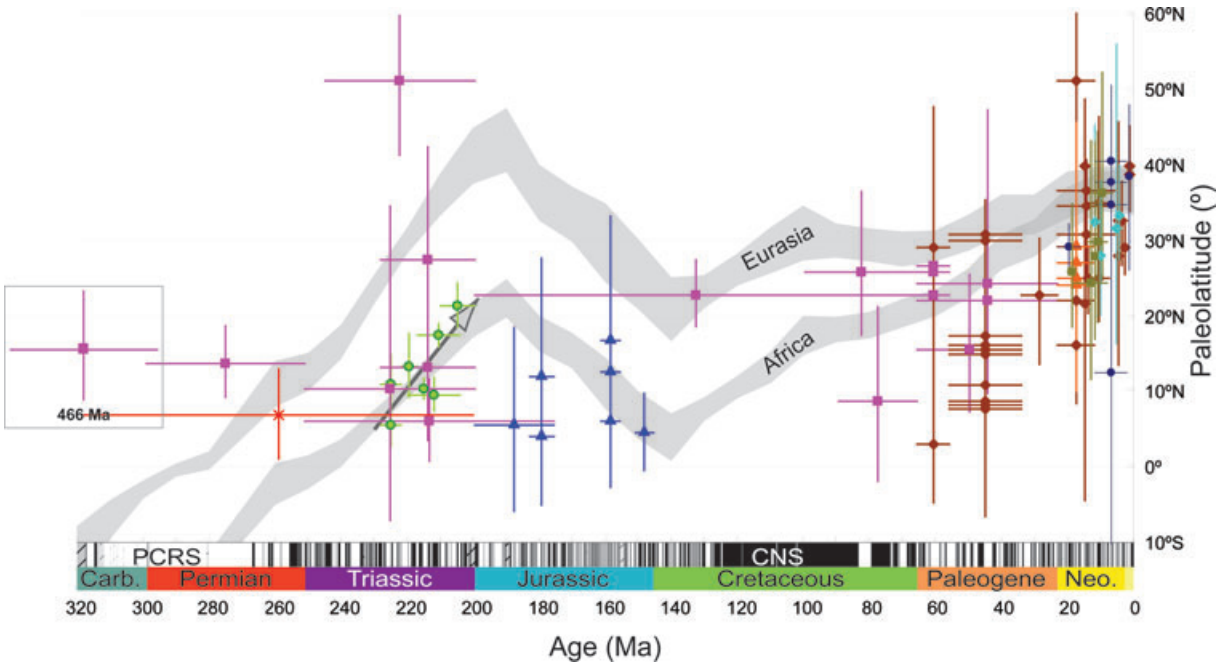


**Figure 10.** Age versus latitute plots of Tauride data from the literature, with tilt correction. Purple squares, Morris & Robertson (1993); red cross, Van der Voo & Van der Kleijn (1970); light green circles, Gallet *et al*. (1992, 1993, 1994, 2000, 2007); blue triangles, Piper *et al*. (2002); red diamonds, Kissel & Poisson (1987) and Kissel *et al*. (1993); orange triangles, van Hinsbergen *et al*. (2010b); dark blue circles, van Hinsbergen *et al*. (2010a); dark green triangles, Gürsoy *et al*. (2003); light blue diamonds, Tatar *et al*. (2002). Grey shaded curves, APW path of Torsvik *et al*. (2008) with its error from 320–0 Ma. Below the curves the magnetic polarity timescale (Ogg *et al*. 2008) is indicated. PCRS, Permo-Carboniferous Reversed Superchrom; CNS, Cretaceous Normal Superchron; Carb., Carboniferous. The data from the magnetostratigraphic studies by Gallet *et al*. (1992, 1993, 1994, 2000, 2007) that are not remagnetized show the same trend as the African path (see arrow). Note that most data have too low inclinations, which is most likely caused by compaction of the sediment and corresponding flattening of the inclination.

is required, for example using the IRM acquisition end-member modelling approach reported here.

The compilation of the post-Mesozoic data sets at first-order confirms the generally accepted conclusion of Kissel *et al*. (1993) that the eastern limb of the Isparta Angle experienced an older clockwise rotation between Eocene and early Miocene time, followed by a counter-clockwise rotation in middle-late Miocene time in the western limb (see also van Hinsbergen *et al*. 2010a). However, as argued above, it is possible that remagnetization occurred during thrusting of the Taurides. If that is true, also the lower Eocene rocks used by Kissel *et al*. (1993) to reconstruct rotations of the central Taurides may have been remagnetized. This implies that the reported rotations of Kissel & Poisson (1986, 1987) and Kissel *et al*. (1993) and of the Ordovician to Eocene sites should be regarded as a minimum value, as they may have been reset during rotation. This would have no serious implications for the timing of clockwise rotation of the eastern limb of the Isparta Angle, as it remains at some time between the early Eocene and early Miocene.

An important implication of an Eocene remagnetization during the early stages of tilting is that the remagnetized declination of our sites could be used to assess the regional rotation pattern of the central Taurides. However, our results do not concur with a regional 40° clockwise rotation. As can be seen in Fig. 2(a), the rotations in the central Taurides are consistently clockwise, with strongly varying amounts of rotation. The results from the Seydişehir section give only $14 \pm 2.7°$ clockwise, and for the Taşkent section even less ($7 \pm 2.8°$), significantly less than the 40° of clockwise rotation concluded by Kissel *et al*. (1993). Only our result for the Fele section gives $56 \pm 9.5°$, not significantly higher than some of the rotations observed by Kissel *et al*. (1993).

The question thus arises whether there is indeed a regional, central Tauride-wide coherent rotation of 40° clockwise. Kissel *et al*. (1993) report two sites from the Eocene around the Ermenek basin in the south, which give significantly different clockwise rotations of 13° and 38°, despite their close vicinity. Add to these sites our information for a varying post-remagnetization rotation and a pattern arises for consistently clockwise rotations, but with strongly varying rotation amounts. These strong, significantly different rotation values suggest that local rotations between sites have played a role. This is not surprising, considering the likely influence of local, thrust-sheet or strike-slip related rotations, superimposed on a regionally coherent rotation of the central Taurides.

## 6 CONCLUSIONS

The results of our palaeomagnetic study on three sections/localities with Carboniferous to Palaeocene sediments from the central Taurides show that the sampled rocks are remagnetized. This conclusion is based on palaeomagnetic results that display reversed directions in the CNS as well as remarkably similar post-tilting palaeolatitudes in all samples, regardless of their age. Remagnetization directions yield both normal and reversed polarities, proving that the remagnetization was not a short and single event, but likely has occurred throughout a longer time interval. We show additional evidence for remagnetization from a novel end-member modelling approach of IRM acquisition curves from the Seydişehir section. The shape of the end-member that we interpret as the magnetite end-member indicates remagnetization. The remagnetization is likely of chemical origin, caused by internal fluids (because of calcite pressure solution), in line with the presence of stylolites and dolomites in the area.

Reversed remagnetization directions and reliable Burdigalian (∼20–16 Ma) data form previous studies bracket the remagnetization event between ∼85 and 20 Ma. Furthermore, the similar palaeolatitudes after tilt correction agree well with the late Cretaceous to Eocene apparent polar wander path and suggest that remagnetization took place during this time span, just prior to or during the early stages of folding. This is confirmed by the fold test and SCI method that were applied to the Seydişehir section, suggesting the acquisition of the remagnetized ChRM direction upon ∼65–68 per cent unfolding. Continuous sedimentation in the Seydişehir area until the Eocene would likely place the remagnetization in this time span.

Comparison of our results to published data shows that the rotation observed in our remagnetized data agrees well with the general and consistently clockwise trend in the central Taurides. The slightly divergent pattern in rotations, however, shows that rotations are not regionally coherent, but are likely and at least in part influenced by local faulting. The post-tilting remagnetization reported by Morris & Robertson (1993) in the southwestern Antalya Nappes, is likely not valid for a number of sites of their study. Interestingly, the Triassic tilt-corrected data of Morris & Robertson (1993) agree very well with rotations found by Gallet *et al*. (1992, 1994, 2000) in Triassic magnetostratigraphic sections. These clockwise rotations coincide with the rotation pattern of the central Taurides, and contrast with the counter-clockwise rotations in Beydağları and the Lycian Nappes. The palaeolatitudes from the Triassic sites also correspond very well to the Triassic African apparent polar wander part. An additional study, for instance using the end-member algorithm on IRM acquisition curves, would be required to re-evaluate the remagnetized nature of the rocks sampled by Morris & Robertson (1993).

## ACKNOWLEDGMENTS

The authors would like to thank Peter Mackintosh for his help preparing the fieldtrips and Ahmet Peynircioğlu, Pınar Ertepınar and Ayten Koç for their help in the field. We would like to thank Robin Topper for measuring several subsets of samples used for this study as a part of his MSc research. The two reviewers, R. Douglas Elmore and Martin Waldhör, are thanked for their very constructive comments. We would also like to thank Martin Waldhör for help with the applied SCI method and the figures he provided (Data S2). The MATLAB modules and an executable can be found online at: http://www.marum.de/Unmixing_magnetic_remanence_curves_without_a_priori_knowledge.html. Spreadsheets and explanation for using the SCI method can be found online at http://www.geo.uni-tuebingen.de/arbeitsgruppen/angewandte-geowissenschaften/geophysik/research.html.

## REFERENCES

Altıner, D., Yılmaz, I.Ö., Özgül, N., Akçar, N., Bayazıtoğlu, M. & Gaziulusoy, Z.E., 1999. High-resolution sequence stratigraphic correlation in the Upper Jurassic (Kimmeridgian)-Upper Cretaceous (Cenomanian) peritidal carbonate deposits (Western Taurides, Turkey), *Geol. J.,* **34,** 139–158.

Andrew, T. & Robertson, A.H.F., 2002. The Beysehir-Hoyran-Hadim Nappes: genesis and emplacement of Mesozoic marginal and oceanic units of the northern Neotethys in southern Turkey, *J. geol. Soc. Lond.,* **159,** 529–543.

Bağcı, U. & Parlak, O., 2009. Petrology of the Tekirova (Antalya) ophiolite (Southern Turkey): evidence for diverse magma generations and their

tectonic implications during Neotethyan-subduction, *Int. J. Earth Sci.,* **98,** 387–405, doi:10.1007/s00531-007-0242-7.

Bassant, P., van Buchem, F.S.P., Strasser, A. & Görür, N., 2005. The stratigraphic architecture and evolution of the Burdigalian carbonate-siliciclastic sedimentary systems of the Mut Basin, Turkey, *Sedimentary Geol.,* **173,** 187–232.

Blumstein, A.M., Elmore, R.D., Engel, M.H., Elliot, C. & Basu, A., 2004. Paleomagnetic dating of burial diagenesis in Mississippian carbonates, Utah, *J. geophys. Res.,* **109,** B04101, doi:10.1029/2003JB002698.

Butler, R.F., 1992. *Paleomagnetism: Magnetic Domains to Geologic Terranes,* Blackwell Scientific Publications, Boston.

Çelik, Ö.F. & Delaloyle, M.F., 2003. Origin of metamorphic soles and their post-kinematic mafic dyke swarms in the Antalya and Lycian ophiolites, SW Turkey, *Geol. J.,* **38,** 235–256.

Çelik, Ö.F., Delaloyle, M.F. & Feraud, G., 2006. Precise $^{40}Ar$–$^{39}Ar$ ages from the metamorphic sole rocks of the Tauride Belt Ophiolites, southern Turkey: implications for the rapid cooling history, *Geol. Mag.,* **143,** 213–227.

Channell, J.E.T. & McCabe, C., 1994. Comparison of magnetic hysteresis parameters of unremagnetized and remagnetized limestones, *J. geophys. Res.,* **99**(B3), 4613–4623.

Çiner, A., Karabıyıkoğlu, M., Monod, O., Deynoux, M. & Tuzcu, S., 2008. Late Cenozoic Sedimentary Evolution of the Antalya Basin, Southern Turkey, *Turkish J. Earth Sci.,* **17,** 1–41.

Collins, A.S. & Robertson, A.H.F., 1998. Processes of Late Cretaceous to Late Miocene episodic thrust-sheet translation in the Lycian Taurides, SW Turkey, *J. geol. Soc. Lond.,* **155,** 759–772.

Creer, K.M., 1962. The dispersion of the geomagnetic field due to secular variation and its determination for remote times from paleomagnetic data, *J. geophys. Res.,* **67**(9), 3461–3476.

Creer, K.M., Irving, E. & Nairn, A.E.M., 1959. Paleomagnetism of the great whin sill, *Geophys. J. R. astr. Soc.,* **2,** 306–323.

Davydov, V., Wardlaw, B.R. & Gradstein, F.M., 2004. The carboniferous period, in *A Geologic Time Scale 2004,* pp. 222–237, eds Gradstein, F. M., Ogg, J.G. & Smith, A.G., Cambridge University Press, Cambridge.

Dean, W.T. & Monod, O., 1970. The Lower Palaeozoic stratigraphy and faunas of the Taurus mountains near Beyşehir, Turkey, *Bull. Br. Museum (Natural History) Geol.,* **19**(8), 411–426.

Dean, W.T., Uyeno, T.T. & Rickards, R.B., 1999. Ordovician and Silurian stratigraphy and trilobites, Taurus Mountains near Kemer, southwestern Turkey, *Geol. Mag.,* **136,** 373–393.

Dekkers, M.J. & Pietersen, H.S., 1992. Magnetic properties of low-Ca fly ash: a rapid tool for Fe-assessment and a proxy for environmental hazard, in *Advanced Cementitious Systems: Mechanisms and Properties,* Vol. **245**, pp. 37–47, eds Glasser, F.P. *et al*., Mat. Res. Soc. Symp. Proc., Material Research Society, Pittsburgh, PA.

Deynoux, M., Çiner, A., Monod, O., Karabıyıkoğlu, M., Manatschal, G. & Tuzcu, S., 2005. Facies architecture and depositional evolution of alluvial fan to fan-delta complexes in the tectonically active Miocene Köprüçay Basin, Isparta Angle, Turkey, *Sedimentary Geol.,* **173,** 315–343.

Dilek, Y. & Whitney, D.L., 1997. Counterclockwise P-T-t trajectory from the metamorphic sole of a Neo-Tethyan ophiolite (Turkey), *Tectonophysics,* **280,** 295–310.

Dilek, Y., Thy, P., Hacker, B.R. & Grundvig, S., 1999. Structure and petrology of Tauride ophiolites and mafic dike intrusions (Turkey): implications for the Neotethyan ocean, *Geol. Soc. Am. Bull.,* **111,** 1192–1216.

Dumont, J.F., Gutnic, M., Marcoux, J., Monod, O. & Poisson, A., 1972. Le Trias des Taurides occidentales (Turquie). Definition du bassin pamphylien: un nouveau domain à ophiolites à la marge externe de la chaine taurique, *Z. Dtsh Geologische Ges.,* **123,** 385–409.

Egli, R., 2004. Characterization of individual rock magnetic components by analysis of remanence curves. 2. Fundamental properties of coercivity distributions, *Phys. Chem. Earth,* **29**(13–14), 851–867.

Elitok, Ö. & Drüppel, K., 2008. Geochemistry and tectonic significance of metamorphic sole rocks beneath the Beysehir–Hoyran ophiolite (SW-Turkey), *Lithos,* **100,** 322–353.

Elmore, R.D., Dulin, S., Engel, M.H. & Parnell, J., 2006. Remagnetization and fluid flow in the Old Red Sandstone along the Great Glen Fault, Scotland, *J. Geochem. Explor.,* **89,** 96–99.

Eris, K.K., Bassant, P. & Ülgen, U.B., 2005. Tectono-stratigraphic evolution of an Early Miocene incised valley-fill (Derinçay Formation) in the Mut Basin, Southern Turkey, *Sedimentary Geol.,* **173,** 151–185.

Evans, M.A., Lewchuk, M.T. & Elmore, R.D., 2003. Strain partitioning of deformation mechanisms in limestones: examining the relationship of strain and anisotropy of magnetic susceptibility (AMS), *J. Struct. Geol.,* **25,** 1525–1549.

Fisher, D.A., 1953. Dispersion on a sphere, *Proc. R. Soc. Lond. A,* **217,** 295–305.

Flecker, R.M., Robertson, A.H.F., Poisson, A. & Müller, C., 1995. Facies and tectonic significance of two contrasting Miocene basins in south coastal Turkey, *Terra Nova,* **7,** 221–232.

Gallet, Y., Besse, J., Krystyn, L., Marcoux, J. & Théveniaut, H., 1992. Magnetostratigraphy of the Late Triassic Bolucektasi Tepe section (southwestern Turkey): implications for changes in magnetic reversal frequency, *Phys. Earth Planet. Inter.,* **73,** 85–108.

Gallet, Y., Besse, J., Krystyn, L., Théveniaut, H. & Marcoux, J., 1993. Magnetostratigraphy of the Kavur Tepe section (southwestern Turkey): a magnetic polarity timescale for the Norian, *Earth planet. Sci. Lett.,* **117,** 443–456.

Gallet, Y., Besse, J., Krystyn, L., Théveniaut, H. & Marcoux, J., 1994. Magnetostratigraphy of the Mayerling section (Austria) and Erenkolu Mezarlik (Turkey) section: improvement of the Carnian (late Triassic) magnetic polarity time scale, *Earth planet. Sci. Lett.,* **125,** 173–191.

Gallet, Y., Besse, J., Krystyn, L. & Marcoux, J., 1996. Norian magnetostratigraphy from the Scheiblkogel section, Austria: constraint on the origin of the Antalya Nappes, Turkey, *Earth planet. Sci. Lett.,* **140**(1–4), 113–122.

Gallet, Y., Besse, J., Krystyn, L., Marcoux, J., Guex, J. & Théveniaut, H., 2000. Magnetostratigraphy of the Kavaalani section (southwestern Turkey): consequence for the origin of the Antalya Calcareous Nappes (Turkey) and for the Norian (Late Triassic) magnetic polarity timescale, *Geophys. Res. Lett.,* **27**(14), 2033–2036.

Gallet, Y., Krystyn, L., Marcoux, J. & Besse, J., 2007. New constraints on the End-Triassic (Upper Norian–Rhaetian) magnetostratigraphy, *Earth planet. Sci. Lett.,* **255,** 458–470.

Gessner, K., Collins, A.S., Ring, U. & Güngör, T., 2004. Structural and thermal history of poly-orogenic basement: U-Pb geochronology of granitoid rocks in the southern Menderes Massif, Western Turkey, *J. geol. Soc. Lond.,* **161,** 93–101.

Glover, C.P. & Robertson, A.H.F., 1998. Neotectonic intersection of the Aegean and Cyprus tectonic arcs: extensional and strike-slip faulting in the Isparta Angle, SW Turkey, *Tectonophysics,* **298,** 103–132.

Gong, Z., Dekkers, M.J., Dinarès-Turell, J. & Mullender, T.A.T., 2008a. Remagnetization mechanism of Lower Cretaceous rocks from the Organyà Basin (Pyrenees, Spain), *Studia Geophys. Geod.,* **52,** 187–210.

Gong, Z., Langereis, C.G. & Mullender, T.A.T., 2008b. The rotation of Iberia during the Aptian and the opening of the Bay of Biscay, *Earth planet. Sci. Lett.,* **273**(1–2), 80–93.

Gong, Z., Dekkers, M.J., Heslop, D. & Mullender, T.A.T., 2009a. End-member modeling of isothermal remanent magnetization (IRM) acquisition curves: a novel approach to diagnose remagnetization, *Geophys. J. Int.,* **178,** 693–701.

Gong, Z., van Hinsbergen, D.J.J. & Dekkers, M.J., 2009b. Diachronous pervasive remagnetization in northern Iberian basins during Cretaceous rotation and extension, *Earth planet. Sci. Lett.,* **284,** 292–301.

Gürsoy, H., Piper, J.D.A. & Tatar, O., 2003. Neotectonic deformation in the western sector of tectonic escape in Anatolia: palaeomagnetic study of the Afyon region, central Turkey, *Tectonophysics,* **374,** 57–79.

Gutnic, M., Monod, O., Poisson, A. & Dumont, J. 1979. Géologie des taurides occidentales (Turquie) (Eds.), *Societé Géologique de France, Mémoir*., **137,** 1–112.

Hayward, A.B., 1984. Sedimentation and basin formation related to ophiolite nappe emplacement, Miocene, SW Turkey, *Sedimentary Geol.,* **71,** 105–129.

Heslop, D. & Dillon, M., 2007. Unmixing magnetic remanence curves without a priori knowledge, *Geophys. J. Int.,* **170,** 556–566.

Heslop, D., McIntosh, G. & Dekkers, M.J., 2004. Using time- and temperature-dependent Preisach models to investigate the limitations of modelling isothermal remanent magnetization acquisition curves with cumulative log Gaussian functions, *Geophys. J. Int.,* **157,** 55–63.

Heslop, D., Von Dobeneck, T. & Höcker, M., 2007. Using non-negative matrix factorization in the "unmixing" of diffuse reflectance spectra, *Marine Geol.,* **241**(1–4), 63–78.

Hetzel, R. & Reischmann, T., 1996. Intrusion age of Pan-African augen gneisses in the southern Menderes Massif and the age of cooling after Alpine ductile extensional deformation, *Geol. Mag.,* **133,** 565–572.

van Hinsbergen, D.J.J., 2010. A key extensional metamorphic complex reviewed and restored: the Menderes Massif of western Turkey, *Earth-Sci. Rev.,* **102,** 60–76.

van Hinsbergen, D.J.J., Dekkers, M.J., Bozkurt, E. & Koopman, M., 2010a. Exhumation with a twist: paleomagnetic constraints on the evolution of the Menderes metamorphic core complex (western Turkey), *Tectonics,* **29**(TC3009), doi:10.1029/2009TC002596.

van Hinsbergen, D.J.J., Dekkers, M.J. & Koç, A., 2010b. Testing Miocene remagnetization of Bey Dağları: timing and amount of Neogene rotations in SW Turkey, *Turkish J. Earth Sci.,* **19,** 123–156, doi:10.3906/yer-0904–1.

van Hinsbergen, D.J.J., Kaymakci, N., Spakman, W. & Torsvik, T.H., 2010c. Reconciling the geological history of western Turkey with plate circuits and mantle tomography, *Earth planet. Sci. Lett.,* **297,** 674–686.

Juteau, T., Nicolas, A., Dubessey, J., Fruchard, J.C. & Bouchez, J.L., 1977. Structural relationships in the Antalya Complex, Turkey: possible model for an oceanic ridge, *Geol. Soc. Am. Bull.,* **88,** 1740–1748.

Katz, B., Elmore, R.D., Cogioni, M. & Ferry, S., 1998. Widespread chemical remagnetization: orogenic fluids or burial diagenesis of clays? *Geology,* **26,** 603–606.

Katz, B., Elmore, R.D., Cogioni, M., Engel, M.H. & Ferry, S., 2000. Associations between burial diagenesis of smectite, chemical remagnetization, and magnetite authigenesis in the Vocontian trough, SE France, *J. geophys. Res.,* **105,** 851–868.

Kaymakci, N., Özçelik, Y., White, S.H. & Van Dijk, P.M. 2009. Tectonostratigraphy of the Çankırı Basin: late Cretaceous to early Miocene evolution of the Neotethyan suture zone in Turkey, in *Collision and Collapse at the Africa-Arabia-Eurasia Subduction Zone,* Vol. 311, pp. 67–106, eds Van Hinsbergen, D.J.J., Edwards, M.A. & Govers, R., Geological Society of London, London.

Kent, D.V., 1985. Thermoviscous remagnetization in some Appalachian limestones, *Geophys. Res. Lett.,* **12,** 805–808.

Khair, K. & Tsokas, G.N., 1999. Nature of the Levantine (eastern Mediterranean) crust from multiple-source Werner deconvoloution of Bouguer gravity anomalies, *J. geophys. Res.,* **104,** 25 469–25 478.

Kirschvink, J.L., 1980. The least-square line and plane and the analysis of paleomagnetic data, *Geophys. J. R. astr. Soc.,* **62,** 699–718.

Kissel, C. & Poisson, A., 1986. Etude paléomagnétique préliminaire des formations néogène du bassin d'Antalya (Taurides occidentales-Turquie), *C.R. Acad. Sci., Paris,* **302,** Serie II(10), 711–716.

Kissel, C. & Poisson, A., 1987. Etude paléomagnétique préliminaire des formations cénozoïques des Bey Dağları (Taurides occidentales, Turquie), *C.R. Acad. Sci., Paris,* **304,** Serie II(8), 343–348.

Kissel, C., Averbuch, O., Frizon de Lamotte, D., Monod, O. & Allerton, S., 1993. First paleomagnetic evidence for a post-Eocene clockwise rotation of the Western Taurides thrust belt east of the Isparta reentrant (Southwestern Turkey), *Earth planet. Sci. Lett.,* **117,** 1–14.

Kosun, E., Poisson, A., Çiner, A., Wernli, R. & Monod, O., 2009. Syntectonic sedimentary evolution of the Miocene Çatallar Basin, southwestern Turkey, *J. Asian Earth Sci.,* **34,** 466–479.

Kröner, A. & Şengör, A.M.C., 1990. Archean and Proterozoic ancestry in late Precambrian to early Paleozoic crustal elements of southern Turkey as revealed by single-zircon dating, *Geology,* **18,** 1186–1190.

Kruiver, P.P., Dekkers, M.J. & Heslop, D., 2001. Quantification of magnetic coercivity components by the analysis of acquisition curves of isothermal remanent magnetisation, *Earth planet. Sci. Lett.,* **189,** 269–276.

Langmuir, D., 1971. Particle size effect on the reaction goethite = hematite + water, *Am. J. Sci.,* **271,** 147–156.

Machel, H.G. & Cavell, P.A., 1999. Low-flux, tectonically-induced squeegee fluid flow ("hot flash") into the Rocky Mountain Foreland Basin, *Bull. Can. Pet. Geol.,* **47,** 510–533.

Mackintosh, P.W. & Robertson, A.H.F., 2009. Structural and sedimentary evidence from the northern margin of the Tauride platform in south central Turkey used to test alternative models of Tethys during Early Mesozoic time, *Tectonophysics,* **473,** 149–172.

McCabe, C. & Elmore, R.D., 1989. The occurence of Late Paleozoic remagnetization in the sedimentary rocks of North America, *Rev. Geophys.,* **27,** 471–494.

McFadden, P.L. & McElhinny, L.W., 1988. The combined analysis of remagnetization circles and direct observations in palaeomagnetism, *Earth planet. Sci. Lett.,* **87,** 161–172.

Meijers, M.J.M., Kaymakcı, N., van Hinsbergen, D.J. J., Langereis, C.G., Stephenson, R.A. & Hippolyte, J.-C., 2010. Late Cretaceous to Paleocene oroclinal bending in the central Pontides (Turkey), *Tectonics,* **29,** TC4016, doi:10.1029/2009TC002620.

Moix, P., Beccaletto, L., Kozur, H.W., Hochard, C., Rosselet, F. & Stampfli, G.M., 2008. A new classification of the Turkish terranes and sutures and its implications for the paleotectonic history of the region, *Tectonophysics,* **451,** 7–39.

Monod, O., 1977. *Recherches geologiques dans le Taurus occidental au sud du Beyşehir (Turquie)*. University of Paris-Sud 'Centre d'Orsay', Paris.

Morris, A. & Robertson, A.H.F., 1993. Miocene remagnetisation of carbonate platform and Antalya Complex units within the Isparta Angle, SW Turkey, *Tectonophysics,* **220,** 243–266.

O'Brien, V.J., Moreland, K.M., Elmore, R.D., Engel, M.H. & Evans, M.A., 2007. Origin of orogenic remagnetizations in Mississippian carbonates, Sawtooth Range, Montana, *J. geophys. Res.,* **112,** B06103, doi:10.1029/2006JB004699.

Ogg, J.G., Agterberg, F.P. & Gradstein, F.M. 2004. The cretaceous period, in *A Geologic Time Scale 2004,* pp. 344–383, eds Gradstein, F.M., Ogg, J.G. & Smith, A.G., Cambridge University Press, Cambridge.

Ogg, J.G., Ogg, G. & Gradstein, F.M. 2008. *The Concise Geologic Time Scale*. Cambridge University Press, Cambridge.

Okay, A.I., 1984. Distribution and characteristics of the northwest Turkish blueschists, in *The Geological Evolution of the Eastern Mediterranean,* Vol. 17, pp. 455–466, eds Dixon, J.E. & Robertson, A.H.F., Geological Society Special Publication, London.

Okay, A.I., Satır, M., Maluski, H., Siyako, M., Monié, P., Metzger, R. & Akyüz, S. 1996. Paleo- and Neo-Tethyan events in northwestern Turkey: geologic and geochronologic constraints, in *The Tectonic Evolution of Asia,* pp. 420–441, eds Yin, A. & Harrison, T.M., Cambridge University Press, Cambridge.

Okay, A.I., Tansel, I. & Tüysüz, O., 2001. Obduction, subduction and collision as reflected in the Upper Cretaceous-Lower Eocene sedimentary record of western Turkey, *Geol. Mag.,* **138**(2), 117–142.

Özer, E., Koç, H. & Özsayar, T.Y., 2004. Stratigraphical evidence for the depression of the northern margin of the Menderes–Tauride Block (Turkey) during the Late Cretaceous, *J. Asian Earth Sci.,* **22,** 401–412.

Özgül, N., 1976. Some geological aspects of the Taurus orogenic belt (Turkey), *Bull. Geol. Soc. Turkey,* **19,** 65–78, (In Turkish).

Özgül, N., 1983. Stratigraphy and tectonic evolution of the Central Taurides, in *Geology of the Taurus Belt*, Int. Symp., Mineral Research and Exploration Inst., 1983 September 26–29, Ankara, pp. 78–90, eds Tekeli, O. & Göncüöglü, Geological Society of Turkey and the Mineral Research and Exploration Institute, Ankara.

Payne, J.L. *et al*, 2007. Erosional truncation of uppermost Permian shallow-marine carbonates and implications for Permian-Triassic boundary events, *Geol. Soc. Am. Bull.,* **119**(7/8), 771–784, doi:10.1130/B26091.1.

Peynircioğlu, A.A. 2005. Micropaleontological Analysis and Facies Evolution across the Tournaisian—Visean Boundary in Aladağ Unit (central Taurides, Turkey), Vol. 90, *MSc thesis*. Middle East Technical University, Ankara.

Piper, J.D.A., Gursoy, H., Tatar, O., Isseven, T. & Kocyigit, A., 2002. Palaeomagnetic evidence for the Gondwanian origin of the Taurides and rotation of the Isparta Angle, southern Turkey, *Geol. J.,* **37,** 317–336.

Poisson, A., Wernli, R., Sagular, E.K. & Temiz, H., 2003a. New data concerning the age of the Aksu Thrust in the south ofthe Aksu valley, Isparta

Angle (SW Turkey): consequences for the Antalya Basin and the Eastern Mediterranean, *Geol. J.,* **38,** 311–327.
Poisson, A., Yagmurlu, F., Bozcu, M. & Sentürk, M., 2003b. New insights on the tectonic setting and evolution around the apex of the Isparta Angle (SW Turkey), *Geol. J.,* **38,** 257–282.
Ricou, L.E., Argyriadis, I. & Marcoux, J., 1975. L'axe calcaire du Taurus, un alignement de fenêtres arabo-africaines sous des nappes radiolaritiques, ophiolitiques et métamorphiques, *Bull. Soc. Géol. France,* **17,** 1024–1043.
Ricou, L.E., Marcoux, J. & Poisson, A., 1979. L'allochtonie des Bey Dağları orientaux. Reconstruction palinspastique des Taurides occidentales, *Bull. Soc. Géol. France,* **11,** 125–133.
Robertson, A.H.F. & Woodcock, N.H., 1981. Alakir Çay group, Antalya Complex, SW Turkey: a deformed Mesozoic carbonate margin, *Sedimentary Geol.,* **30,** 95–131.
Robertson, A.H.F., Ustaomer, T., Pickett, E.A., Collins, A.S., Andrew, T. & Dixon, J.E., 2004. Testing models of Late Palaeozoic-Early Mesozoic orogeny in Western Turkey: support for an evolving open-Tethys model, *J. geol. Soc. Lond.,* **161,** 501–511.
Robertson, A.H.F., Parlak, O. & Ustaömer, T., 2009. Melange genesis and ophiolite emplacement related to subduction of the northern margin of the Tauride-Anatolide continent, central and western Turkey, in *Collision and Collapse at the Africa-Arabia-Eurasia Subduction Zone,* Vol. 311, pp. 9–66, eds Van Hinsbergen, D.J.J., Edwards, M.A. & Govers, R., Geological Society of London, London.
Satır, M. & Friedrichsen, H., 1986. The origin and evolution of the Menderes Massif, W-Turkey: a rubidium/strontium and oxygen isotope study, *Geologische Rundsch.,* **75,** 703–714.
Şenel, M. *et al.,* 2001. Geological map of Turkey, 1:500.000. Ankara, Turkey, MTA.
Şengör, A.M.C., 1984. *The Cimmeride Orogenic System and the Tectonics of Eurasia*, Geological Society of America, Boulder, CO, 82pp.
Şengör, A.M.C. & Yilmaz, Y., 1981. Tethyan evolution of Turkey: a plate tectonic approach, *Tectonophysics,* **75**(3–4), 181–241.
Şengör, A.M.C., Altıner, D., Cin, A., Ustaömer, T. & Hsu, K.J. 1988. Origin and assembly of the Tethyside orogenic collage at the expense of Gondwana Land, in *Gondwana and Tethys,* Vol. 37, pp. 119–181, eds Audley-Charles, M.G. & Hallam, A., Geological Society Special Publications, London.
Shipunov, S.V., 1997. Synfolding magnetization: detection, testing and geological applications, *Geophys. J. Int.,* **130**(2), 405–410.
Stampfli, G.M. & Borel, G.D., 2002. A plate tectonic model for the Paleozoic and Mesozoic constrained by dynamic plate boundaries and restored synthetic oceanic isochrons, *Earth planet. Sci. Lett.,* **196**(1–2), 17–33.
Tatar, O., Gürsoy, H. & Piper, J.D.A., 2002. Differential neotectonic rotations in Anatolia and the Tauride Arc: palaeomagnetic investigation of the Erenlerdag Volcanic Omplex and Isparta volcanic district, south-central Turkey, *J. geol. Soc. Lond.,* **159,** 281–294.
Tauxe, L. & Kent, D.V. 2004. A simplified statistical model for the geomagnetic field and the detection of shallow bias in paleomagnetic inclinations: was the ancient magnetic field dipolar? in *Timescales of the Paleomagnetic Field,* Vol. 145, pp. 101–115, Channell, J.E.T., Kent, D.V., Lowrie, W. & Meert, J.G., AGU Geophysical Monograph, Washington, DC.
Tauxe, L. & Watson, G.S., 1994. The foldtest: an eigen analysis approach, *Earth planet. Sci. Lett.,* **122,** 331–341.
Tauxe, L., Kodama, K.P. & Kent, D.V., 2008. Testing corrections for paleomagnetic inclination error in sedimentary rocks: a comparative approach, *Phys. Earth planet. Inter.,* **169,** 152–165.
Torsvik, T.H., Muller, R.D., Van Der Voo, R., Steinberger, B. & Gaina, C., 2008. Global plate motion frames: toward a unified model, *Rev. Geophys.,* **46,** RG3004, doi:10.1029/2007RG000227.
Tüysüz, O., 1999. Geology of the Cretaceous sedimentary basins of the Western Pontides, *Geol. J.,* **34,** 75–93.
Van Der Voo, R. & Van der Kleijn, P.H., 1970. The complex NRM of the Permo-Carboniferous Bademli redbeds (Tauride chains, southern Turkey), *Geol. Mijnb.,* **49**(5), 391–395.
Van Velzen, A.J. & Zijderveld, J.D.A., 1995. Effects of weathering on single domain magnetite in early Pliocene marls, *Geophys. J. Int.,* **121,** 267–278.
Vandamme, D., 1994. A new method to determine paleosecular variation, *Phys. Earth planet. Inter.,* **85,** 131–142.
Waldhör, M. & Appel, E., 2006. Intersections of remanence small circles: new tools to improve data processing and interpretation in palaeomagnetism, *Geophys. J. Int.,* **166**(1), 33–45.
Wardlaw, B.R., Davydov, V. & Gradstein, F.M. 2004. The permian period, in *A Geologic Time Scale 2004,* pp. 249–264, eds Gradstein, F.M., Ogg, J.G. & Smith, A.G., Cambridge University Press, Cambridge.
Weltje, G.J., 1997. End-member modeling of compositional data: numerical-statistical algorithms for solving the explicit mixing problem, *Math. Geol.,* **29,** 503–546.
Yalınız, K.M., Göncüoglu, M.C. & Özkan-Altıner, S., 2000. Formation and emplacement ages of the SSZ-type Neotethyan ophiolites in Central Anatolia, Turkey: palaeotectonic implications, *Geol. J.,* **35,** 53–68.
Yapp, C.J., 1983. Effects of AlOOH-FeOOH solid solution on goethite-hematite equilibrium, *Clays Clay Miner.,* **31,** 239–240.
Yılmaz, I.Ö. & Altıner, D., 2006. Cyclic paleokarst surfaces in Aptian peritidal carbonate successions (Taurides, southwest Turkey): internal structure and response to mid-Aptian sea-level fall, *Cretaceous Res.,* **27,** 814–827.
Zegers, T.E., Dekkers, M.J. & Bailly, S., 2003. Late Carboniferous to Permian remagnetization of Devonian limestones in the Ardennes: role of temperature, fluids, and deformation, *J. geophys. Res.,* **108**(B7), 2357, doi:10.1029/2002JB002213.
Zijderveld, J.D.A., 1967. A. C. demagnetization of rocks: analysis of results, in *Methods in Palaeomagnetism,* pp. 254–286, eds Collinson, D.W., Creer, K.M. & Runcorn, S.K., Elsevier, Amsterdam.

## SUPPORTING INFORMATION

Additional Supporting Information may be found in the online version of this article:

**Data S1.** Schematic sedimentary log of the Seydişehir section.
**Data S2.** Results of the fold test (a–c) for the Seydişehir section (without TT7, TT28, TT0, TT3 and TT32). Equal area projection of the sites means before (a) and after (b) correction for bedding orientation, (c) results of a non-parametric fold test as 500 bootstrapped examples of the first eigenvalues ($\tau_1$) upon progressive untilting. Above the diagram the 95 per cent bootstrap error is given; the error margin does not include full (100 per cent) untilting and hence there is no positive fold test. Best clustering is around 70 per cent untilting, indicating acquisition of the NRM in an early stage of tilting. Results of the SCI method for the Seydişehir section shown for all sites except TT7 and TT28. Results excluding TT0, TT3 and TT32 are also shown in the figure. (d) ChRM directions *in situ* (red squares) and tilt corrected (blue squares) per site. Large diamonds represent Fisherian mean of all included sites. Black dots represent bedding poles of all included sites, (e) all small circles, their intersections and best-fit SCI-estimates (Shipnov's method) with and without the outliers (sites TT0, TT3 and TT32), (f) contour plot (equal area projection) of fit parameter *S* of final SCI-estimate for a circular x–y-grid with nodes every 0.01. Figs (d)–(f) were kindly provided by Waldhör (personal communication, 2010).

Please note: Wiley-Blackwell are not responsible for the content or functionality of any supporting materials supplied by the authors. Any queries (other than missing material) should be directed to the corresponding author for the article.